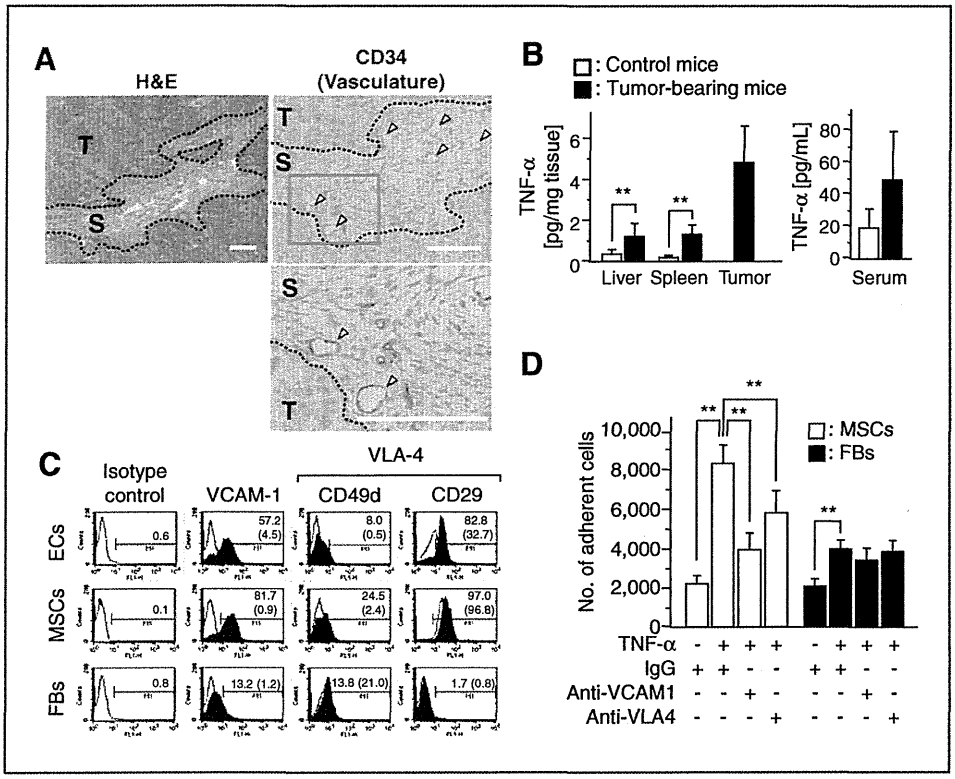

Figure 3. A, sections represent hematoxylin and eosin (H&E) staining (top left), the $CD34^+$ blood vessels/endothelial cells in tumor tissues (top right), the high-power field of view (bottom). Data shown are from 1 representative experiment of 3 carried out. Scale bar, 100 μm. S, stroma; T, tumor. B, specimens of tumor, liver, spleen, and blood were collected from control and tumor-bearing mice. TNF-α levels in tissue homogenates and serum were assayed by ELISA. *, $P < 0.05$; **, $P < 0.01$. C, MSCs, endothelial cells (EC), and fibroblasts were cultured with TNF-α (10 ng/mL) for 6 hours. Cells were labeled with FITC-conjugated antibodies and analyzed by flow cytometry (filled histogram). Rat isotype antibodies IgG1 and IgG2a served as respective controls (open histograms). Values represent the percentage of positive cells after TNF-α stimulation, and values in parentheses represent the percentage of positive cells without TNF-α stimulation. D, endothelial cells were cultured to confluence on fibronectin-coated 96-well plates. Then, MSCs or fibroblasts (1×10^4) were added to cultured endothelial cells. MSCs and endothelial cells were pretreated with the following substances: TNF-α (10 ng/mL), anti-VCAM-1, VLA-4 (10 μg/mL), or isotype control IgG. Values are mean ± SD. **, $P < 0.01$ ($n = 6$ per cell type).

that has been proposed for endothelial cell regulation of leukocyte infiltration in inflammatory tissues. Leukocyte-endothelial adhesion involves dynamic interactions between leukocytes and endothelial cells, and involves multiple steps. These steps must be precisely orchestrated to ensure a rapid response with minimal damage to healthy tissue (15). Interactions between leukocytes and the endothelium are mediated by several families of adhesion molecules, each of which participates in a different phase of the process. The surface expression and activation of these molecules during an inflammatory response is tightly controlled under normal conditions. Inflammatory cytokines including IL-1 and TNF-α involve induction of adhesion molecules. In our experimental settings, although other inflammatory cytokine levels including IL-1 and IL-6 were low (data not shown), significant production of TNF-α was observed. We do not clearly know the source of TNF-α in the tumor at this time, and that our *in vitro* data only suggest that the stroma is the primary source.

As we expected, TNF-α enabled MSCs to adhere to endothelial cells through induction of the expression of adhesion molecules, including VCAM-1 and VLA-4. It is generally considered that VCAM-1 on activated endothelium interacts with the VLA-4 on the leukocyte in the model of leukocyte–endothelial cell adhesion. At first, we speculated that VLA-4 on MSCs plays the same important role as leukocytes. Although both VCAM-1 and VLA-4 on endothelium were efficiently induced by TNF-α stimulation, TNF-α–induced expression of VCAM-1 on MSCs is much stronger than that of VLA-4. Furthermore, MSC–EC adhesion was more effectively inhibited by anti-VCAM-1 antibody as compared with the anti-VLA-4 antibody. On the basis of these results, although VLA-4 on MSC have also related to the MSC-EC adhesion, we thought that VCAM-1 on MSC has more important implications for this adhesion. Once MSCs circulate in the bloodstream, adhesion to endothelial cells is the first step in accumulation in tumors. TNF-α exerts its biologic functions through activating the NF-κB signaling pathway. NF-κB is a major cell survival signal that is antiapoptotic. MSC accumulation was significantly decreased through parthenolide inhibition of NF-κB activity. Although several studies have shown that mitogen-activated protein kinase (MAPK) phosphorylation by growth factors are involved in MSC migration (16, 17), parthenolide did not inhibit MAPK phosphorylation (data not shown). Therefore, at least parthenolide treatment did not affect in migration ability of

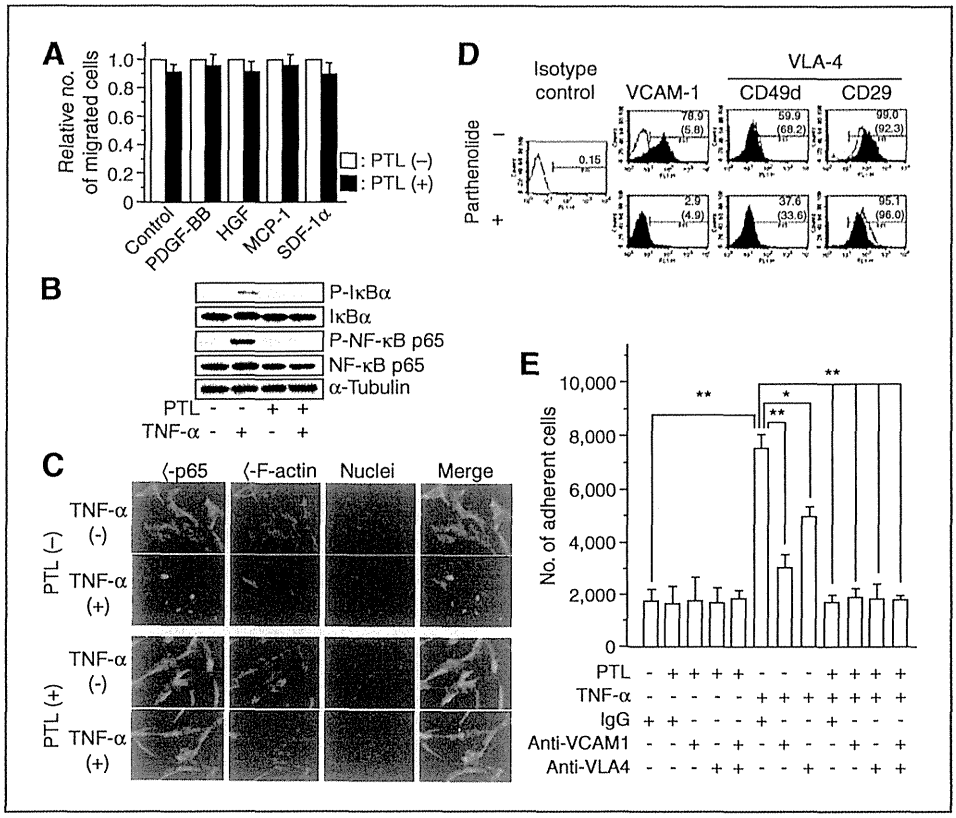

Figure 4. Effect of parthenolide (PTL) on MSC migration and adhesion. A, serum-starved and parthenolide-treated MSCs were added to the upper wells and serum-free medium supplemented with PDGF-BB (10 ng/mL), HGF (30 ng/mL), MCP-1 (100 ng/mL), or SDF-1α (150 ng/mL) was added to the lower wells. Treatment with medium alone (DMEM/F-12) was a negative control and treatment with 30% FBS was the positive control. Values are expressed by relative number of cells compared with respective controls (without pretreatment with parthenolide). B, to assess the inhibitory effect of parthenolide on NF-κB phosphorylation, parthenolide-treated MSCs were stimulated with recombinat TNF-α for 3 minutes, and cellular extracts were prepared for Western blotting. C, to monitor the inhibitory effect of parthenolide on NF-κB activation, immunofluorescent analysis of NF-κB p65 nuclear translocation was conducted as described in Materials and Methods with an Alexa Fluor 488–conjugated specific antibody (green). Actin filaments were labeled with Alexa Fluor 546–conjugated phalloidin (red); nuclei were stained with DRAQ-5 dye (blue). Objective magnification, ×40. D, effect of parthenolide treatment on TNF-α–induced expression of adhesion molecules was analyzed by flow cytometry. Parthenolide-treated MSCs were cultured with TNF-α (10 ng/mL) for 6 hours. Cells were labeled with FITC-conjugated antibodies and analyzed by flow cytometry (filled histogram). Rat isotype antibodies IgG1 and IgG2a served as respective controls (open histograms). Values represent the percentage of positive cells after TNF-α stimulation, and values in parentheses represent the percentage of positive cells without TNF-α stimulation. E, MSCs (1×10^4) were added to endothelial cells that had been cultured to confluence on fibronectin-coated 96-well plates. MSCs and endothelial cells were pretreated with the following substances: parthenolide (5 μmol/L), TNF-α (10 ng/mL), anti-VCAM-1, VLA-4 (10 μg/mL), or isotype control IgG. Values are expressed as mean ± SD ($n = 6$). *, $P < 0.05$ and **, $P < 0.01$.

MSCs toward growth factors from tumors in this experimental settings. Nevertheless, MSC accumulation was significantly decreased through parthenolide inhibition of NF-κB activity. We did not show histologic evidence in the experiments using parthenolide. However, we show that parthenolide does not inhibit luciferase activity *in vitro* (and thus does not seem to be toxic), and that therefore the effect observed *in vivo* should be an effect on recruitment. Although we focused on the function of TNF-α in this study, other inflammatory cytokines including IL-1β and IFN-γ also have ability to induce VCAM-1 expression in target cells (18), and may be involved in MSC accumulation.

TNF-α is a major inflammatory cytokine that plays important roles in diverse cellular events, such as cell survival, proliferation, differentiation, and death. Numerous reports have shown that TNF-α levels in serum are increased in patients with cancer (19, 20), and TNF-α is also related closely to the tumor progression including metastasis. For example, TNF-α intensely induces IL-6 and MCP-1 from cancer-associated fibroblasts and normal fibroblastic cells and has indirect influences on generation of prometastatic microenvironment (21). Furthermore, TNF-α is also released in cardiac infarction, during acute coronary syndromes, and in chronic heart failure; MSCs also accumulate at the site of cardiac infarction (22, 23). These results indicated that proinflammatory cytokines promote homing of stem cells in the heart and that these cytokines have a positive effect on cardiac regeneration. Therefore, activation with TNF-α is one of the critically important steps for MSC accumulation. Moreover, MSC-based tissue-targeted strategies may be adapted for various inflammatory diseases.

In MSC-based cancer-targeted gene therapies, it is thought that therapeutic efficacy is directly linked with accumulation efficiency of MSCs at tumor sites. Our results suggested that combination use of NF-κB inhibitors, including bortezomib, or TNF-α blocking agents, such as infliximab, reduces the

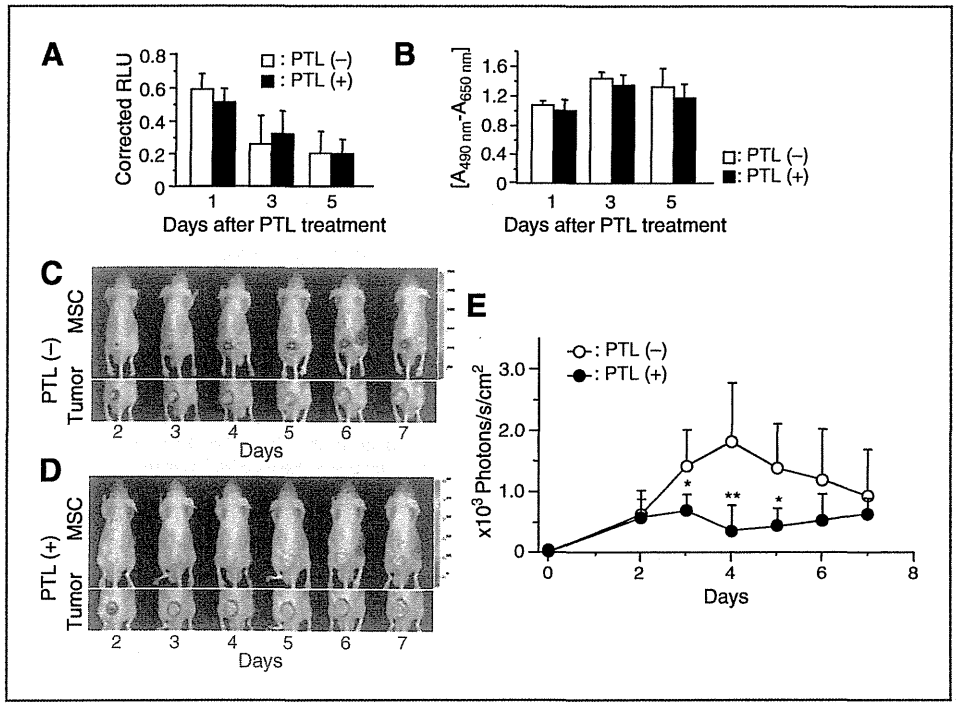

Figure 5. *In vivo* imaging of NF-κB–suppressed MSC accumulation at tumor sites. A, luciferase-expressing MSCs were cultured with parthenolide for 6 hours and luciferase assays were periodically conducted. Values are expressed as mean ± SD ($n = 4$ each). RLU, relative light unit. B, cell viability of parthenolide (PTL)-treated luciferase-expressing MSCs was also examined by XTT assays. Values are expressed as mean ± SD ($n = 4$ each). C, luciferase-expressing MSCs without parthenolide treatment were injected into tumor-bearing mice through the left ventricular cavity and IVIS imaging was periodically conducted. Each data shown are from 1 representative experiment of 8 carried out. D, luciferase-expressing MSCs with parthenolide treatment were injected into tumor-bearing mice and IVIS imaging was periodically conducted. Imaging was conducted as described earlier. Each data shown are from 1 representative experiment of 8 carried out. E, bioluminescent intensity at tumor sites was quantified using analysis software. The data are expressed as mean ± SD ($n = 8$ each). *, $P < 0.05$; **, $P < 0.01$ compared with a group of parthenolide (–) at the same time.

therapeutic efficacy of gene-modified MSCs due to inhibition of the accumulation steps. In contrast, tumor-specific TNF-α–inducing agents would be useful in enhancing therapeutic efficacy, thus further research is required in identifying such agents to more effective therapeutic strategies.

In conclusion, the present study shows that NF-κB activation through TNF-α stimulation and VCAM-1/VLA-4–mediated MSC-EC adhesion may be an important element in MSC accumulation. Although MSCs are useful as cellular vehicles for cancer-targeted gene therapy, past studies have shown that increased MSC accumulation is needed to enhance therapeutic efficacy. Thus, methodology for the enhancement of MSC accumulation should be developed and our findings suggest a solution.

Disclosure of Potential Conflicts of Interest

No potential conflicts of interest were disclosed.

Authors' Contributions

Conception and design: R. Uchibori, H. Mizukami, K. Ozawa
Development of methodology: M. Urabe
Acquisition of data (provided animals, acquired and managed patients, provided facilities, etc.): R. Uchibori
Analysis and interpretation of data (e.g., statistical analysis, biostatistics, computational analysis): R. Uchibori, H. Mizukami, A. Kume
Writing, review, and/or revision of the manuscript: R. Uchibori, M. Urabe, A. Kume
Administrative, technical, or material support (i.e., reporting or organizing data, constructing databases): T. Tsukahara, H. Mizuguchi, Y. Saga, K. Ozawa
Study supervision: M. Urabe, A. Kume, K. Ozawa

Acknowledgments

The authors thank Miyoko Mitsu for her encouragement and technical support.

Grant Support

This work was supported by Grant-in-Aid for Scientific Research (KAKENHI) from the Ministry of Education, Culture, Sports, Science and Technology (21390296 to K. Ozawa), and The Research Award to Jichi Medical School Graduate Student (to R. Uchibori).

The costs of publication of this article were defrayed in part by the payment of page charges. This article must therefore be hereby marked *advertisement* in accordance with 18 U.S.C. Section 1734 solely to indicate this fact.

Received January 13, 2012; revised August 30, 2012; accepted September 11, 2012; published OnlineFirst October 12, 2012.

References

1. Studeny M, Marini FC, Champlin RE, Zompetta C, Fidler IJ, Andreeff M. Bone marrow-derived mesenchymal stem cells as vehicles for interferon-beta delivery into tumors. Cancer Res 2002;62:3603–8.

2. Studeny M, Marini FC, Dembinski JL, Zompetta C, Cabreira-Hansen M, Bekele BN, et al. Mesenchymal stem cells: potential precursors for tumor stroma and targeted-delivery vehicles for anticancer agents. J Natl Cancer Inst 2004;96:1593–603.
3. Nakamizo A, Marini F, Amano T, Khan A, Studeny M, Gumin J, et al. Human bone marrow-derived mesenchymal stem cells in the treatment of gliomas. Cancer Res 2005;65:3307–18.
4. Chen X, Lin X, Zhao J, Shi W, Zhang H, Wang Y, et al. A tumor-selective biotherapy with prolonged impact on established metastases based on cytokine gene-engineered MSCs. Mol Ther 2008;16:749–56.
5. Xin H, Kanehira M, Mizuguchi H, Hayakawa T, Kikuchi T, Nukiwa T, et al. Targeted delivery of CX3CL1 to multiple lung tumors by mesenchymal stem cells. Stem Cells 2007;25:1618–26.
6. Uchibori R, Okada T, Ito T, Urabe M, Mizukami H, Kume A, et al. Retroviral vector-producing mesenchymal stem cells for targeted suicide cancer gene therapy. J Gene Med 2009;11:373–81.
7. Dwyer RM, Potter-Beirne SM, Harrington KA, Lowery AJ, Hennessy E, Murphy JM, et al. Monocyte chemotactic protein-1 secreted by primary breast tumors stimulates migration of mesenchymal stem cells. Clin Cancer Res 2007;13:5020–7.
8. Mizuguchi H, Kay MA. Efficient construction of a recombinant adenovirus vector by an improved *in vitro* ligation method. Hum Gene Ther 1998;9:2577–83.
9. Mizuguchi H, Kay MA. A simple method for constructing E1- and E1/E4-deleted recombinant adenoviral vectors. Hum Gene Ther 1999;10:2013–7.
10. Koizumi N, Mizuguchi H, Utoguchi N, Watanabe Y, Hayakawa T. Generation of fiber-modified adenovirus vectors containing heterologous peptides in both the HI loop and C terminus of the fiber knob. J Gene Med 2003;5:267–76.
11. Mittereder N, March KL, Trapnell BC. Evaluation of the concentration and bioactivity of adenovirus vectors for gene therapy. J Virol 1996;70:7498–509.
12. Coussens LM, Werb Z. Inflammation and cancer. Nature 2002;420:860–7.
13. Honczarenko M, Le Y, Swierkowski M, Ghiran I, Glodek AM, Silberstein LE. Human bone marrow stromal cells express a distinct set of biologically functional chemokine receptors. Stem Cells 2006;24:1030–41.
14. Rüster B, Göttig S, Ludwig RJ, Bistrian R, Müller S, Seifried E, et al. Mesenchymal stem cells display coordinated rolling and adhesion behavior on endothelial cells. Blood 2006;108:3938–44.
15. Butcher EC. Leukocyte-endothelial cell recognition: three (or more) steps to specificity and diversity. Cell 1991;67:1033–6.
16. Coffelt SB, Marini FC, Watson K, Zwezdaryk KJ, Dembinski JL, LaMarcad HL, et al. The pro-inflammatory peptide LL-37 promotes ovarian tumor progression through recruitment of multipotent mesenchymal stromal cells. Proc Natl Acad Sci U S A 2009;106:3806–11.
17. Zhang A, Wang Y, Ye Z, Xie H, Zhou L, Zheng S. Mechanism of TNF-α-induced migration and hepatocyte growth factor production in human mesenchymal stem cells. J Cell Biochem 2010;111:469–75.
18. Hosokawa Y, Hosokawa I, Ozaki K, Nakae H, Matsuo T. Cytokines differentially regulate ICAM-1 and VCAM-1 expression on human gingival fibroblasts. Clin Exp Immunol 2006;144:494–502.
19. Ferrajoli A, Keating MJ, Manshouri T, Giles FJ, Dey A, Estrov Z, et al. The clinical significance of tumor necrosis factor-alpha plasma level in patients having chronic lymphocytic leukemia. Blood 2002;100:1215–9.
20. Ahmed MI, Salahy EE, Fayed ST, El-Hefnawy NG, Khalifa A. Human papillomavirus infection among Egyptian females with cervical carcinoma: relationship to spontaneous apoptosis and TNF-alpha. Clin Biochem 2001;34:491–8.
21. Mueller L, von Seggern L, Schumacher J, Goumas F, Wilms C, Braun F, et al. TNF-alpha similarly induces IL-6 and MCP-1 in fibroblasts from colorectal liver metastases and normal liver fibroblasts. Biochem Biophys Res Commun 2010;397:586–91.
22. Shake JG, Gruber PJ, Baumgartner WA, Senechal G, Meyers J, Redmond JM, et al. Mesenchymal stem cell implantation in a swine myocardial infarct model: engraftment and functional effects. Ann Thorac Surg 2002;73:1919–25.
23. Pittenger MF, Martin BJ. Mesenchymal stem cells and their potential as cardiac therapeutics. Circ Res 2004;95:9–20.

Gene Therapy (2012) 19, 476–482

www.nature.com/gt

ORIGINAL ARTICLE

Interleukin-10 expression induced by adeno-associated virus vector suppresses proteinuria in Zucker obese rats

M Ogura[1,2], M Urabe[1], T Akimoto[2], A Onishi[1,2], C Ito[2], T Ito[3], T Tsukahara[1], H Mizukami[1], A Kume[1], S Muto[2], E Kusano[2] and K Ozawa[1]

Varying degrees of metabolic abnormalities mediated by chronic inflammation are implicated in the chronic glomerular injuries associated with obesity. Interleukin (IL)-10, a pleiotropic cytokine, exerts anti-inflammatory effects in numerous biological settings. In the present study, we explored the biological benefits of adeno-associated virus (AAV) vector-mediated sustained IL-10 expression against the pathological renal characteristics observed in Zucker fatty rats (ZFRs). We injected an AAV vector, encoding rat IL-10 or enhanced green fluorescent protein (GFP) into male ZFRs at 5 weeks of age. Subsequently, the renal pathophysiological changes were analyzed. Persistent IL-10 expression significantly reduced the urinary protein excretion of ZFRs compared with GFP expression (47.1 ± 11.6 mg per mg·creatinine versus 88.8 ± 30.0 mg per mg·creatinine, $P<0.01$). The serum levels of IL-10 negatively correlated with the urinary protein in AAV-treated rats ($r=-0.78$, $P<0.01$). Renal hypertrophy, increased widths in the glomerular basement membrane, and the lack of uniformity and regularity of the foot process of the visceral glomerular epithelial cells of ZFRs were significantly blunted by IL-10 expression. IL-10 also abrogated the downregulation of glomerular nephrin observed in ZFRs treated with the GFP vector. Our findings provide insights into the potential benefit of the anti-inflammatory effects of IL-10 on the overall management of glomerulopathy induced by the metabolic disorders associated with obesity.
Gene Therapy (2012) **19**, 476–482; doi:10.1038/gt.2011.183; published online 24 November 2011

Keywords: obesity; nephrin; glomerular hyperfiltration; glomerular epithelial cells; glucose intolerance

INTRODUCTION

Numerous pathophysiological disorders have been demonstrated to be related to obesity.[1] Not exceptionally, accumulating evidence also suggests a role for obesity in the development of chronic kidney disease.[2–4] The renal effects of obesity in humans and experimental animals include both functional and morphological adaptations, such as an increased glomerular filtration rate, increased renal blood flow, and renal hypertrophy with focal segmental glomerulosclerosis.[5–7] Although the qualitative and quantitative information about the pathogenesis of the glomerulopathy associated with obesity remains to be delineated, varying degrees of metabolic abnormalities appear to be involved. Indeed, hyperinsulinemia resulted in the stimulation of the synthesis of insulin-like growth factors, and the upregulation of transforming growth factor-β1 by elevated serum leptin has been implicated in the chronic glomerulopathy associated with obesity.[8,9] Moreover, hyperlipidemia may also promote glomerulosclerosis through mechanisms in which engagement of lipoprotein receptors on mesangial cells, oxidative cellular injury, macrophage chemotaxis and accelerated synthesis of fibrogenic cytokines are involved.[10]

Interleukin (IL)-10 is a multifunctional cytokine with anti-inflammatory properties.[11] Accumulating evidence suggests potential roles for IL-10 in the management of several pathophysiological disorders, including obesity. Indeed, IL-10 has been shown to not only reduce cholesterol levels, but also to improve the insulin resistance in experimental animal models.[12,13] Moreover, it has also been reported that obese patients and subjects with metabolic syndrome have a lower level of serum IL-10 than healthy normal subjects.[14] These observations led us to consider the therapeutic potential of modulating inflammation by IL-10 in the overall management of obese patients.

In the present study, we evaluated the effects of IL-10 on the renal characteristics of Zucker fatty (Zucker-fa/fa) rats, which have recently been focused on as an experimental animal model of renal injuries mediated by obesity-associated metabolic disorders.[7,15,16] The biological efficiency of the systemic administration of recombinant IL-10 seems to be insufficient because of the immediate decrease resulting from its short bioactive half-life.[17] Instead, we have transferred the gene encoding IL-10 using an adeno-associated virus (AAV) vector, as these vectors can be used to transduce skeletal muscle, thereby inducing the systemic and sustained expression of potentially therapeutic proteins following a single intramuscular administration.[12,18]

RESULTS

The expression of IL-10 in Zucker rats

Our first series of experiments verified the integrity of our vectors in the Zucker-fa/fa rats. The serum concentrations of IL-10 in the rats were determined at 5, 10, 15, 20 and 25 weeks after the initial treatments, which included the administration of phosphate buffer saline (PBS) and transductions of the recombinant AAV type 1-based vector carrying the rat IL-10 (AAV–IL-10) or control-enhanced green fluorescent protein gene (AAV–GFP). As shown in Figure 1,

[1]Division of Genetic Therapeutics, Center for Molecular Medicine, Jichi Medical University, Shimotsuke, Japan; [2]Division of Nephrology, Department of Medicine, Jichi Medical University, Shimotsuke, Japan and [3]Division of Cardiovascular Medicine, Department of Medicine, Jichi Medical University, Shimotsuke, Japan
Correspondence: Dr M Ogura, Division of Nephrology, Department of Internal Medicine, Jichi Medical School, 3311-1 Yakushiji, Shimotsuke-Shi, Tochigi 329-0498, Japan.
E-mail: m-ogura@jichi.ac.jp
Received 25 May 2011; revised 21 September 2011; accepted 17 October 2011; published online 24 November 2011

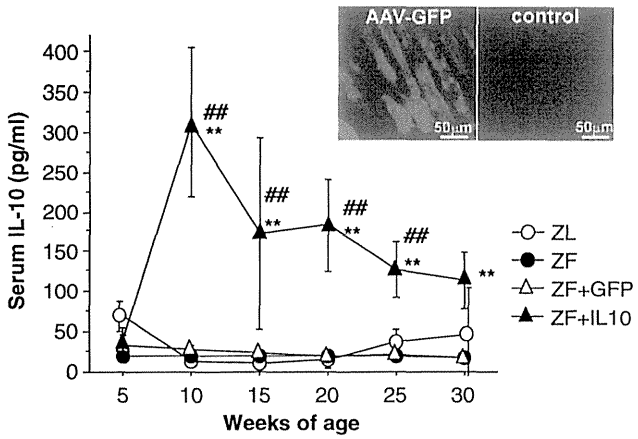

Figure 1 The longitudinal changes in serum concentrations of IL-10 at 5, 10, 15, 20 and 25 weeks after the initial sham treatments (PBS alone), and transductions of AAV–IL-10 or AAV–GFP into the Zucker fa/fa rats or lean littermates. Inset: an analysis of the cryostat sections of the anterior tibial muscles injected with AAV–GFP or PBS (control). The immunofluorescence analyses performed 10 weeks post-vector injections revealed ubiquitous GFP expression within the muscle tissue, thus suggesting efficient gene transduction by the AAV vectors. Scale bar is indicated in each panel. The data are the means ± s.d. (n=6). $^{**}P<0.01$ versus ZF and ZF+GFP groups; $^{\#\#}P<0.01$ versus the value at 5 weeks of age.

statistically significant increases in serum IL-10 were confirmed in Zucker-fa/fa rats administered AAV–IL-10 (sham Zucker-fa/fa rats administered PBS (ZF)+IL-10), whereas the levels in Zucker-fa/fa rats administered AAV–GFP (ZF+GFP), ZF and control Zucker lean littermates (Zucker +/+) administered PBS (ZL) were comparable. The levels of IL-10 in ZF+IL-10 were about 12-fold higher at week 5, and an average of 5-fold higher than ZF, ZF+GFP and ZL groups at 25 weeks after the initial treatments.

The effects of IL-10 on clinical and laboratory characteristics

The body weights of all rats were increased during the observation period. Although the degree of the increases was significantly higher in the Zucker-fa/fa rats than in the ZL rats, the mean body weights of ZF, ZF+GFP and ZF+IL-10 at each time point were comparable (Figure 2a). Similarly, the food consumption of the Zucker-fa/fa rats was significantly greater than that of the ZL, although there were no significant differences in the amount of food intake in the three Zucker-fa/fa rat groups (Figure 2b). On the other hand, the serum levels of total cholesterol (Tcho) and triglycerides (TG) were significantly higher in Zucker-fa/fa rats compared with ZL throughout the observation period. However, in the ZF+IL-10, the serum Tcho was significantly lower than those in the ZF and ZF+GFP (Figure 2c). Similar trends were also confirmed in the longitudinal changes in the serum TG. As shown in Figure 2d, Zucker-fa/fa rats had significantly higher serum TG than their lean littermates; however, the expression of IL-10 seemed to negatively affect the level of TG. At 30 weeks of age, these parameters negatively correlated with the IL-10 level in the Zucker-fa/fa rats with PBS or AAV treatment (Figures 2e and f). During the observation period, no significant difference in the systolic blood pressure was observed in the Zucker-fa/fa rats treated with PBS or the AAV, although there was a trend for the systolic blood pressure in the ZL to be higher than that of all of the Zucker-fa/fa rats (data not shown).

We next analyzed the effect of IL-10 on the parameters related to the glucose metabolism. As shown in Table 1, the fasting blood glucose levels of Zucker-fa/fa rats were significantly higher at 10 weeks after the administration of the vector with GFP or PBS administration compared with the lean littermates. At 30 weeks of age, we determined the blood hemoglobin A1c (HbA1c) and serum immuno-reactive insulin levels. As shown in Figure 3a, the transduction of IL-10 reversed the increase in the levels of HbA1c that was confirmed in ZF and ZF+GFP rats, thus suggesting that IL-10 might have a role in improving the disturbance of the fed-state glucose metabolism in the Zucker fa/fa rats. Indeed, the fed state serum insulin level was significantly elevated in ZF+IL-10 rats compared with the other groups, whereas the levels of fasting serum insulin in the Zucker-fa/fa rats were comparable (Figure 3b).

The effects of IL-10 on renal characteristics

We also explored the effects of IL-10 on the renal characteristics of the obese rats. As shown in Figure 4a, all three groups of obese rats (ZF, ZF+GFP and ZF+IL-10) demonstrated a gradual increase in urinary protein in a time-dependent manner, and the urinary protein level in the ZF and ZF+GFP finally increased up to 102.2 ± 21.9 and 88.8 ± 30.0 mg per mg·creatinine, respectively. At 30 weeks of age, the urinary protein in the ZF+IL-10 (47.1 ± 11.6 mg per mg·creatinine) was significantly lower than in the other Zucker-fa/fa rats groups ($P<0.01$). Moreover, the serum levels of IL-10 negatively correlated with the urinary protein level in Zucker-fa/fa rats ($r=-0.88$, $P<0.01$, $n=17$; Figure 4b). During the observation period, the creatinine clearance (Ccr) in obese rats without IL-10 was significantly increased at both 25 and 30 weeks of age (Figure 4c). There was also a negative correlation between the serum IL-10 level and Ccr ($r=-0.65$, $P<0.01$, $n=15$; Figure 4d).

Figure 5 shows the anatomical and morphological effects of IL-10 on the Zucker-fa/fa rats. All three groups of Zucker-fa/fa rats had significantly higher kidney weights than the ZL at 30 weeks of age. However, the expression of IL-10 caused a significant decrease in the kidney weight when compared with the ZF and ZF+GFP (1.70 ± 0.13 g versus 1.86 ± 0.12 g, $P<0.05$, and 1.85 ± 0.09 g, $P<0.05$, respectively; Figure 5a). When viewed under a light microscope, there were no apparent histological changes compatible with glomerulosclerosis and cellular infiltrations within the glomerulus in any of the subjects; however, the Zucker-fa/fa rats had a larger area of glomeruli than the ZL, which was significantly reduced by the persistent expression of IL-10 in the ZF+IL-10 (Figures 5b and c). Transmission electron microscopy showed the hyperplastic glomerular basement membrane (GBM) and prominent foot process effacement in ZF and ZF+GFP (Figure 5b), but these changes seemed to be prevented or reversed in the ZF+IL-10. Indeed, there were significant differences in the mean width of the GBM between the ZF+IL-10 and the other two groups of Zucker-fa/fa rats (Figure 5d). The lack of uniformity and regularity of the foot process demonstrated by scanning electron microscopic was remarkable in the ZF and ZF+GFP, but this was not observed in the ZF+IL-10 and ZL (Figure 5b).

The effects of IL-10 on the expression of nephrin within the glomeruli of Zucker-fa/fa rats

To determine the potential mechanisms of the counter-effect of IL-10 on the changes in the renal characteristics in the Zucker-fa/fa rats, we evaluated the effects of IL-10 on the expression of nephrin within glomeruli. As shown in Figure 6, the glomerular nephrin expressions in Zucker fa/fa rats treated with PBS or AAV–GFP were significantly diminished compared with that of lean littermates, and the transduction of IL-10 apparently reversed the reduced expression of nephrin within glomeruli that was observed in the Zucker-fa/fa rats (Figure 6).

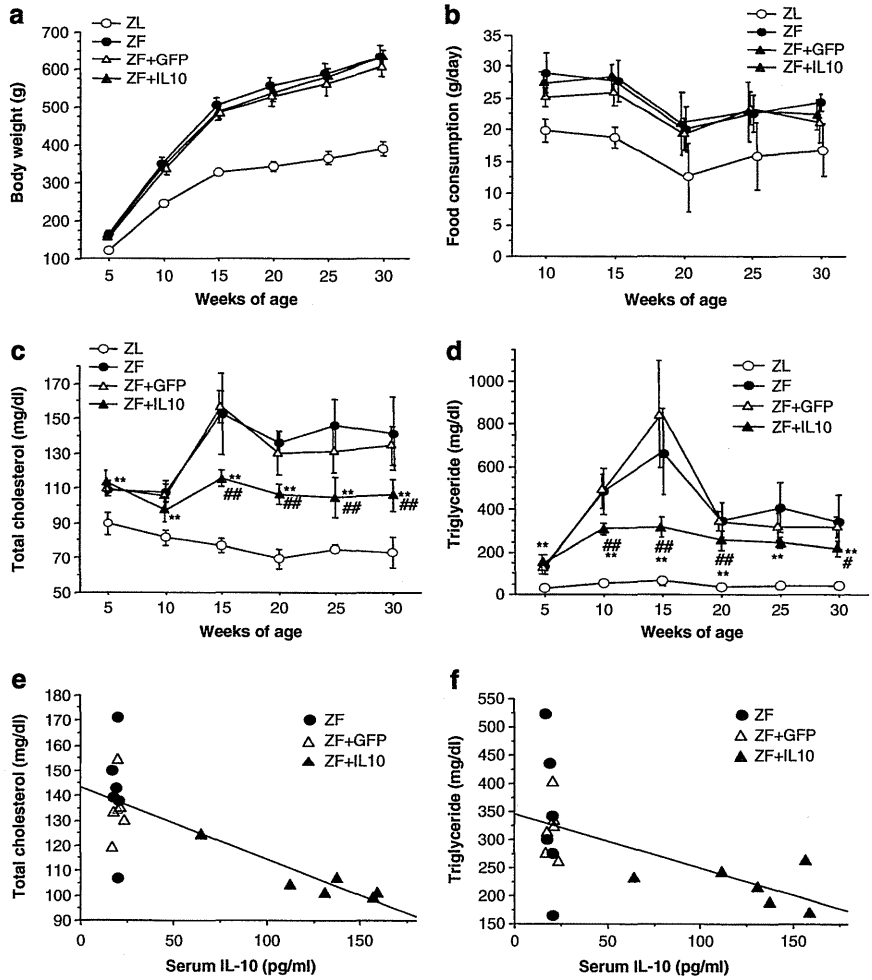

Figure 2 The changes in the body weights (**a**), food consumption (**b**), serum Tcho (**c**) and serum TG (**d**). The body weights and food consumption were significantly higher in obese rats than in lean littermates at each point time. Note that the body weights and the food consumption in the three groups of obese rats were comparable, whereas the serum Tcho and TG levels were significantly lower than those in the ZF and ZF+GFP groups. The data are the means ± s.d. (n=6). $^{**}P<0.01$ versus the control; $^{\#}P<0.05$, $^{\#\#}P<0.01$ versus ZF and ZF+GFP groups. The relationships between IL-10 and Tcho (**e**) and TG (**f**) were also evaluated (groups: ZF, ZF+GFP and ZF+IL-10; n=6 per group; r=−0.77, $P<0.01$ and r=−0.77, $P<0.01$, respectively).

Table 1 Changes in FBS in Zucker fa/fa rats and age-matched control lean littermates

Age (weeks)	*ZL*	*ZF*	*ZF+GFP*	*ZF+IL-10*
10	127.2±12.1	157.5±21.0[a]	175.5±19.6[a]	175.8±24.5[a]
20	120.2±7.3	126.3±13.5	129.2±11.5	139.2±22.1[a]
30	108.8±14.3	118.7±16.3	135.3±20.0[a]	126.8±10.8[a]

Abbreviations: FBS, fasting blood glucose; GFP, green fluorescent protein; IL, interleukin; ZF, sham Zucker-fa/fa rats administered PBS; ZL, Zucker lean littermates (Zucker +/+) administered PBS. [a]$P<0.05$ versus ZL.

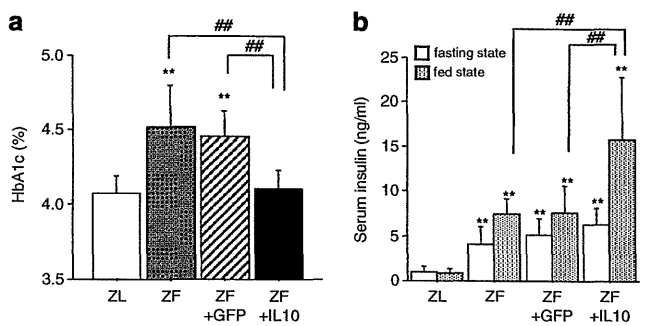

Figure 3 The effect of the IL-10 expression on the level of blood HbA1c (**a**) and serum immunoreactive insulin (**b**). The data were determined with blood samples obtained from rats at 30 weeks of age. $^{**}P<0.01$ versus the control and $^{\#\#}P<0.01$, respectively.

DISCUSSION

The present study clearly demonstrates for the first time that IL-10, delivered by an AAV vector, suppresses the changes in renal characteristics in obese rats, including the increase in urinary protein, elevated Ccr, glomerular hypertrophy and the decreased glomerular expression of nephrin, without affecting the body weight and food intake of the rats. These results suggest the potential benefits of IL-10 in the management of obese subjects with renal pathophysiological abnormalities.

Numerous studies have focused on the abnormalities in lipid metabolism as a potential mechanism underlying various types of glomerular injuries, and the treatment of hyperlipidemia has been shown to reduce the excretion of urinary proteins and to decrease the

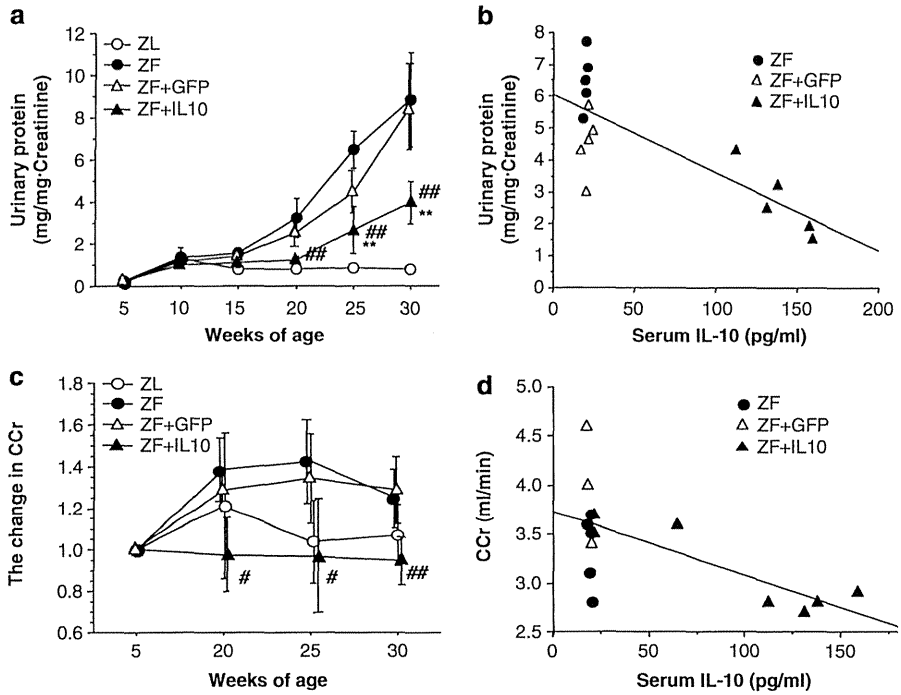

Figure 4 The effects of the IL-10 expression on urinary protein excretion (**a**) and the changes in the Ccr (**c**) in the ZF (●), ZF+GFP (▲), ZF+IL-10 (▲) and ZL (○) rats. The data are the means ± s.d. (n=5–6). $^{**}P<0.01$ versus the controls; $^{\#}P<0.05$, $^{\#\#}P<0.01$ versus ZF or ZF+GFP groups. The relationship between IL-10 and the urinary protein excretion (**b**) or the change in the Ccr (**d**) in the obese rats (groups: ZF, ZF+GFP or ZF+IL-10; n=5–6 per group; r=−0.78, $P<0.01$ and r=−0.65, $P<0.01$, respectively).

glomerular injury characterized by mesangial matrix expansion and focal segmental glomerulosclerosis, which are typical of Zucker fa/fa rats at about 60 weeks of age, without any changes in glomerular hemodynamic function.[7,10,16,19] As such renal structural alterations seem to be relatively nonspecific and may represent part of a common final pathway,[15] we focused on the changes in renal characteristics that precede the development of mesangial matrix expansion and focal segmental glomerulosclerosis. Consistently, the histological analyses of our Zucker fa/fa rats performed at 30 weeks of age failed to demonstrate such glomerular lesions. Instead, glomerular hypertrophy, an increase in the widths of the GBM and the elevation of Ccr due to presumable glomerular hyperfiltration, which have all been implicated in hyperglycemia and are considered to be early events followed by diabetic glomerulosclerosis among diabetic subjects,[20–22] were observed.

These findings might not be surprising, as abnormal glucose metabolism characterized by mild hyperglycemia, as well as hyperinsulinemia and insulin resistance, are alternative metabolic characteristics of Zucker fa/fa rats.[7,15,23] Obviously, this was also the case with the present study. Of note, IL-10 seems to improve the disturbed fed-state glucose metabolism of the Zucker fa/fa rats, as the HbA1c in ZF-IL-10 rats was significantly decreased compared with the rest of the obese groups. The recovery from advanced insulin resistance is unlikely to be implicated in these rats. Instead, the accelerated increase in serum insulin seems to be involved in the countervailing effect of IL-10 on the glucose intolerance. Such an increase in serum insulin may be attributable to a change in the metabolic clearance or altered sensitivity to blood glucose. Alternatively, IL-10 might stimulate pancreatic β-cell function.[24] Although the elevation of serum insulin seemed to be necessary for glycemic control among our obese animals, one may argue that this might have adverse consequences on the renal tissue, and thus, might contribute to the development of a wide range of glomerular and interstitial injuries associated with disturbed glucose metabolism.

Indeed, it has been shown that hyperinsulinemia pleiotropically affects the kidney tissue through various pathways.[8,9,25] Nevertheless, renal pathophysiological evaluations failed to confirm the adverse effect of hyperinsulinemia in ZF-IL10 rats. Our results suggest that the biological significance of the improvement in glucose intolerance, mediated by the further increase in serum insulin induced by IL-10, on the renal characteristics of Zucker fa/fa rats should exceed that of hyperinsulinemia. Otherwise, an alternative process independent of the regulation of obesity-related metabolic disturbance might be involved in the countervailing effect of IL-10 on the renal pathophysiological characteristics among our obese animals.

Whether the glomerular morphological changes demonstrated in the present study cause or contribute to the presumable development of mesangial matrix expansion and focal segmental glomerulosclerosis in Zucker-fa/fa rats, which have been demonstrated to have abnormal lipid metabolism at ages older than 30 weeks,[7,10,16,19] remains to be determined. However, the fact that there were significant decreases in the serum levels of Tcho and TG in the ZF+IL-10 rats led us to consider that the early phase of the changes in the renal characteristics of Zucker fa/fa rats might be modulated, at least in part, by IL-10 through the reduction of Tcho and TG. Although the course of the etiological linkage between IL-10 and TG remains to be delineated, previous data suggest that IL-10 might have a direct effect on the cholesterol metabolism through the suppression of the hydroxymethylglutaryl-CoA reductase expression, thereby lowering the Tcho level.[12]

A hyperplastic GBM is often accompanied by changes in the visceral glomerular epithelial cells, that is, podocytes, and a progressive loss of podocyte foot processes associates with narrowing of the filtration slits, whereas the number of podocytes decreases with the increase in

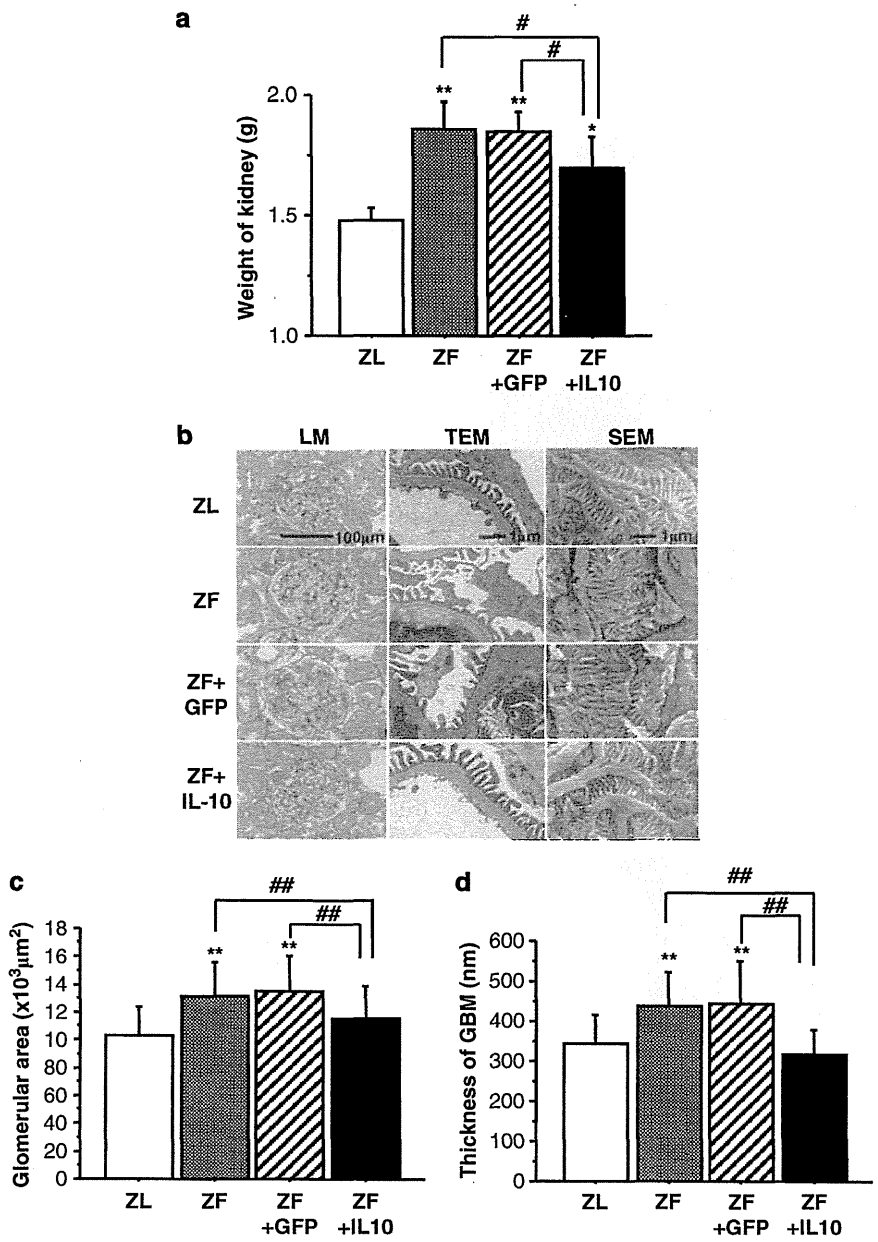

Figure 5 The effects of IL-10 expression on the renal morphological changes in ZFRs. (**a**) The changes in the weights of the kidneys of ZF (black hatched box), ZF+GFP (black striped box), ZF+IL-10 (black box) and ZL (white box) rats. The results were presented as means ± s.d. (n=5). $^{*}P<0.05$, $^{**}P<0.01$, versus the controls; $^{\#}P<0.05$ versus the ZF and ZF+GFP groups. (**b**) Representative photomicrographs of periodic acid-Schiff-stained light microscopic, transmission electron microscopy and scanning electron microscopic views. The scale bars are shown in the panel for the control lean littermates. (**c**) The differences in the glomerular area of the ZF (black hatched box), ZFtGFP (black striped box), ZFtIL-10 (black box) and ZL (white box) rats. (**d**) The differences in the width of the GBM of ZF (black hatched box), ZFtGFP (black striped box), ZFtIL-10 (black box) and ZL (white box) rats. The results are presented as the means ± s.d. $^{**}P<0.01$ versus the controls; $^{\#\#}P<0.01$ versus the ZF and ZF ± GFP groups.

urinary protein excretion.[26,27] Although the precise number of podocytes was not quantified in the present study, such pathogenic processes were likely modulated by IL-10, as the prominent foot process effacement associated with the hyperplastic GBM, and the lack of uniformity and regularity of the foot process confirmed in ZF and ZF-GFP were recovered in ZF+IL-10. Moreover, IL-10 remarkably blunted the reduced glomerular expression of nephrin, which has been located to the slit diaphragm of glomerular podocytes, where it acts as a renal ultrafilter barrier function.[28] Although the mechanism leading to the downregulation of glomerular nephrin in our rats is not well characterized, the potential role of reactive oxygen species, and particularly, the balance of lipid peroxidase, was recently proposed to account for the decrease in nephrin mRNA in experimental glomerulopathy.[29] Therefore, it is reasonable to consider that IL-10 should directly or indirectly modulate such pathophysiological processes within our obese subjects.

Although the present study provides information regarding the effects of IL-10 on the renal characteristics of the Zucker fa/fa rats, our results should be interpreted within the context of the study's limitations. First, the number of animals included in each group was small, implying that the study may be underpowered for the evaluation of several parameters, and selection bias may also be present. Indeed, our

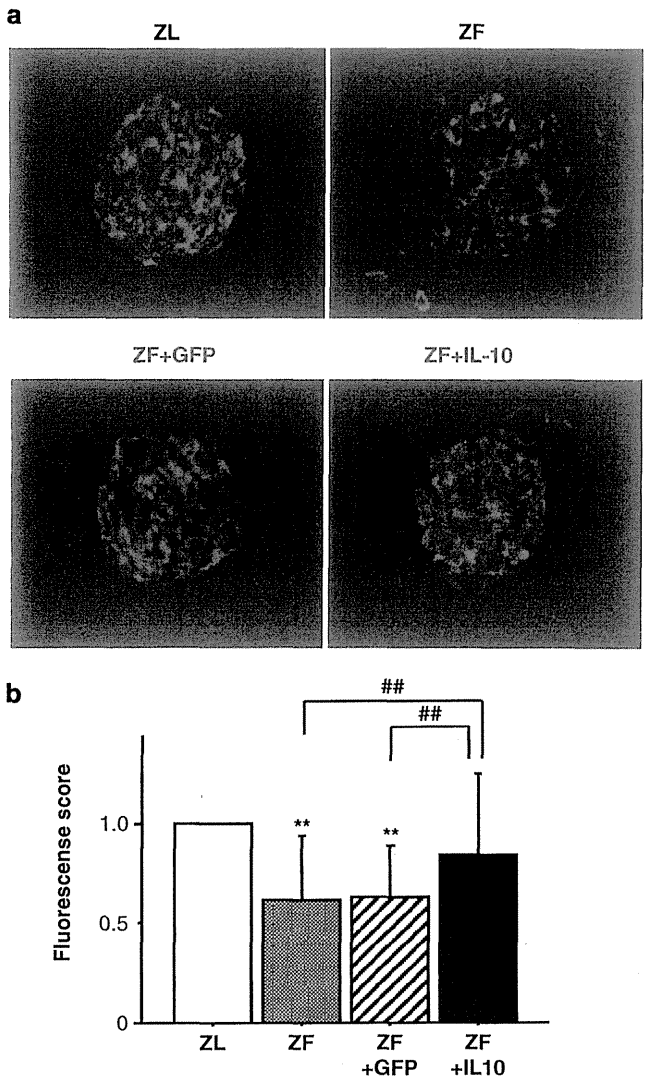

Figure 6 Immunofluorescent staining of glomerular nephrin from ZFRs and control littermates. (**a**) Representative microscopic views are shown. (**b**) The fluorescence intensity of each view was also quantified using arbitrary units. $^{**}P<0.01$ versus control littermates; $n=6$; $^{\#\#}P<0.01$ versus the ZF and ZF+GFP groups.

findings, demonstrating that the mean body weights and the food consumption levels of each of the obese groups, might have been underestimated, as it has been reported that IL-10 could attenuate the changes in food intake and energy expenditure in the experimental rat model of acute inflammatory disturbance associated with bacterial infection.[30] It may be interesting to determine whether the IL-10 treatment applied to our obese rats affected their glucose and lipid metabolism without inducing any change in their body weight and food consumption. Whether our findings remain true when the number of subjects is increased should be evaluated in greater detail in a future study.

In summary, AAV vector-mediated IL-10 gene transfer into the Zucker fa/fa rats could introduce efficient and stable IL-10 expression, resulting in the marked reduction of urinary protein excretion. These changes were associated with the recovery of renal structural alterations. Our observations indicate the presence of complex interactions between the changes in the renal characteristics of Zucker fa/fa rats and the inflammatory cascade, as well as the potential benefit of the anti-inflammatory effects of IL-10 in the overall management of glomerulopathy mediated by obesity-related metabolic disorders.

METHODS

AAV vector production

DNA encoding rat IL-10 was PCR-amplified from rat splenocyte complementary DNA as described previously, using the primers 5′-GCACGAGAGCCAC AACGCa-3′ and 5′-GATTTGAGTACGATCCATTTATTCAAAACGAGGAT-3′.[18] For efficient transgene expression in the skeletal muscle, we constructed a recombinant AAV type 1 vector, which carried the *IL-10* gene or *GFP* gene, controlled by the modified chicken β-actin promoter with the cytomegalovirus posttranscriptional regulatory element (a generous gift from Dr Thomas Hope, Infectious Disease Laboratory, Salk Institute). AAV vectors were prepared according to the previously described three-plasmid transfection adenovirus-free protocol, with minor modification to use the active gassing system.[18,31] Briefly, 60% confluent human embryonic kidney 293 cells incubated in a large culture vessels were co-transfected with the proviral transgene plasmid, AAV-1 chimeric helper plasmid (p1RepCap), and the adenoviral helper plasmid pAdeno (Avigen Inc., Alameda, CA, USA).[31] The crude viral lysates were purified by two rounds of CsCl in a two-tier centrifugation. The titer of the viral stock was determined against plasmid standards by using dot blot hybridization, after which the stock was diluted in PBS before injection.

Animal model and experimental design

All animal procedures were approved by the Jichi Medical University ethics committee and were performed in accordance with the National Institutes of Health Guide for the Care and Use of Laboratory Animals. Male Zucker-fa/fa and Zucker +/+ rats were obtained from Japan SLC Inc (Shizuoka, Japan). Animals were housed in a temperature and humidity controlled room, and standard rat chow (CE-2, Clea Japan, Inc., Tokyo, Japan) and water were available *ad libitum*. Five-week-old male Zucker-fa/fa rats were randomly divided into three groups ($n=6$ in each group): that is, ZF, ZF+GFP and ZF+IL-10. Control lean littermates administered PBS (ZL) were also included in the study. Under ether anesthesia, the PBS buffer or AAV vectors in PBS were injected into the bilateral anterior tibial muscles of the rats (200 μl per site, 1×10^{11} genome copies per rat). For each animal, body weight and food consumption were measured at 5, 10, 15, 20, 25 and 30 weeks of age. Urinary samples were collected in metabolic sampling bottles over 24 h. Blood samples were collected by tail clipping under ether anesthesia after the rats had fasted for 16 h. In some circumstances, morning blood samples were also collected to determine the fed-state blood glucose and serum immunoreactive insulin levels. The serum levels of Tcho (Cholesterol C-test; Wako Chemicals, Tokyo, Japan), TG (L-Type TG H Kit; Wako Chemicals) and IL-10 (Quantikine ELISA Kit; R&D systems, Minneapolis, MN, USA) were determined according to the manufacturer's instructions. The levels of glucose (Shino-Test, Tokyo, Japan) and HbA1c (RAPIDIA Auto HbA1c-L; Fujirebio, Inc., Tokyo, Japan) were determined with whole blood samples. The immunoreactive serum insulin level was determined using a commercial radioimmunoassay kit (Rat insulin RIA kit; Linco Research, Inc., St Charles, MO, USA) with rat insulin as the standard. Systolic blood pressure was measured by the non-invasive tail-cuff method using a manometer–tachometer system (MK-2000, Muromachi Kikai, Tokyo, Japan). The amount of urinary protein excretion for 24 h was determined with TP-HR II Wako reagent (Wako Chemicals). Serum creatinine and urinary creatinine were measured with the creatinine reagent (Alfresa Pharma Corporation, Osaka, Japan), using an automated analyzer (Hitachi-7180, Hitachi High-Technologies, Tokyo, Japan). We calculated the Ccr using the following equation: Ccr (ml min^{-1})=urinary creatinine (mg dl^{-1}) × urine flow rate (ml min^{-1})/serum creatinine (mg dl^{-1}).

Light microscopy

At 30 weeks of age, the anesthetized rats were perfused with 100 ml of saline. For evaluation of light microscopic findings, the kidneys were fixed in 10% paraformaldehyde in PBS (pH 7.4) and finally embedded in paraffin, sectioned, and analyzed for histology. Then, 3-μm sections were subjected to periodic acid-Schiff staining. The mean glomerular tuft volume was determined by the

images from 50 consecutive glomerular cross sections, which were collected for each of the histological sections using an Olympus BX50 light microscope (Olympus, Tokyo, Japan). The area of each glomerular profile was measured manually by tracing the glomerular outline on a computer screen, and the size of each area was calculated by computerized morphometry (Image-Pro plus, Media Cybernetics, Inc., Bethesda, MD, USA). The measurements were performed in a blinded fashion.

Electron microscopy

For transmission electron microscopy, tissues of the left kidneys fixed with 2.5% glutaraldehyde in phosphate buffer (pH 7.4) were postfixed in 2% osmium tetroxide for 2 h at 4 °C. Then, samples were dehydrated in a graded series of ethanol solutions at room temperature, and embedded in Quetol 812 (Nisshin EM Co., Tokyo, Japan). Thin sections of 80 nm were contrasted with 4% uranyl acetate for 15 min and subsequently stained with lead citrate for 5 min at room temperature. Samples were finally examined using a transmission electron microscope (H-7500, Hitachi High-Technologies). The mean width of the GBM was determined by the images of 100 consecutive glomerular sections obtained from two subjects in each group. For scanning electron microscopic examination, small pieces of the kidney cortex were fixed in 2.5% glutaraldehyde in sodium cacodylate buffer (pH 7.4) for 2 h, and subsequently postfixed in 1% osmium tetroxide. Specimens were then dehydrated in a series of ethanols of increasing concentrations, and critical point dried. Once mounted onto specimen holders and desiccated, the samples were sputter-coated with a layer of gold and examined with a S-4300 scanning electron microscope (Hitachi High-Technologies), and images were collected at standard settings.

Immunofluorescent staining

The analysis of nephrin expression in the renal cortex was performed using an immunofluorescence technique. The snap-frozen sections of 3 μm, fixed in 1% formaldehyde and blocked in 5% normal goat serum, were incubated with rabbit anti-nephrin primary antibodies (Immuno-biological Laboratories Co., Ltd., Gunma, Japan) and washed twice with PBS. Subsequently, sections were also incubated with Alexa Fluor 488-conjugated anti-rabbit antibodies (Invitrogen, Carlsbad, CA, USA). Stained sections were examined using a PROVIS AX-80 optical microscope (Olympus). The results were calculated as the intensity of fluorescence within the glomerular tuft by using the Image J 1.42q software package (National Institutes of Mental Health, Bethesda, MD, USA). On average, over 30 randomly selected hilar glomerular tuft cross-sections were assessed per rat.

Statistical analysis

The results were expressed as the means ± s.d. of the mean. The data were analyzed by an analysis of variance combined with Fisher's protected least significant difference. Differences with $P<0.05$ were considered to be statistically significant. The correlation test was used to measure the association between two variables, if appropriate.

CONFLICT OF INTEREST

The authors declare no conflict of interest.

ACKNOWLEDGEMENTS

Part of the work presented in the original manuscript was presented in abstract in the Renal Week 2009 (Annual Meeting of the American Society of Nephrology). We sincerely thank Takashi Yashiro for conducting the electron microscopy studies, and Tom Kouki for his technical assistance in tissue processing for histological and ultrastructural studies.

1 Kambham N, Markowitz GS, Valeri M, Lin J, D'Agati VD. Obesity-related glomerulopathy: an emerging epidemic. *Kidney Int* 2001; **39**: 1498–1509.
2 Ramirez SP, McClellan W, Port FK, Hsu SIH. Risk factors for proteinuria in a large, multiracial, Southeast Asian population. *J Am Soc Nephrol* 2002; **1**: 1907–1917.
3 Iseki K, Ikemiya K, Kinjo K, Inoue T, Iseki C, Takishita S. Body mass index and the risk of development of end-stage renal disease in a screened cohort. *Kidney Int* 2004; **65**: 1870–1876.
4 Hallan S, de Mutsert R, Carlsen S, Dekker FW, Aasarod K, Holmen J. Obesity, smoking, and physical inactivity as risk factors for CKD: are men more vulnerable? *Am J Kidney Dis* 2006; **47**: 396–405.
5 Chagnac A, Weinstein T, Herman M, Hirsh J, Gafter U, Ori Y. The effects of weight loss on renal function in patients with severe obesity. *J Am Soc Nephrol* 2003; **14**: 1480–1486.
6 Chen HM, Li SJ, Chen HP, Wang QW, Li LS, Liu ZH. Obesity-related glomerulopathy in China: a case series of 90 patients. *Am J Kidney Dis* 2008; **52**: 58–65.
7 Kasiske BL, Cleary MP, O'Donnell MP, Keane WF. Effects of genetic obesity on renal structure and function in the Zucker rat. *J Lab Clin Med* 1985; **106**: 598–604.
8 Frystyk J, Skjaerbaek C, Vestbo E, Fisker S, Orskov H. Circulating levels of free insulin-like growth factors in obese subjects: the impact of type 2 diabetes. *Diabetes Metab Res Rev* 1999; **15**: 314–322.
9 Wolf G, Hamann A, Han DC, Helmchen U, Thaiss F, Ziyadeh FN *et al.* Leptin stimulates proliferation and TGF-beta expression in renal glomerular endothelial cells. potential role in glomerulosclerosis. *Kidney Int* 1999; **56**: 860–872.
10 Keane WF. Lipids and the kidney. *Kidney Int* 1994; **46**: 910–920.
11 Mu W, Ouyang X, Agarwal A, Zhang L, Long DA, Cruz PE *et al.* IL-10 suppresses chemokines, inflammation, and fibrosis in a model of chronic renal disease. *J Am Soc Nephrol* 2005; **16**: 3651–3660.
12 Yoshioka T, Okada T, Maeda Y, Ikeda U, Shimpo M, Nomoto T *et al.* Adeno-associated virus vector-mediated interleukin-10 gene transfer inhibits atherosclerosis in apolipoprotein E-deficient mice. *Gene Therapy* 2004; **11**: 1772–1779.
13 Hong EG, Ko HJ, Cho YR, Kim HJ, Ma Z, Yu TY *et al.* Interleukin-10 prevents diet-induced insulin resistance by attenuating macrophage and cytokine response in skeletal muscle. *Diabetes* 2009; **58**: 2525–2535.
14 Esposito K, Pontillo A, Giugliano F, Giugliano G, Marfella R, Nicoletti G *et al.* Association of low interleukin-10 levels with the metabolic syndrome in obese women. *J Clin Endocrinol Metab* 2003; **88**: 1055–1058.
15 Coimbra TM, Janssen U, Grone HJ, Ostendorf T, Kunter U, Schmidt H *et al.* Early events leading to renal injury in obese Zucker (fatty) rats with type II diabetes. *Kidney Int* 2000; **57**: 167–182.
16 Kasiske BL, O'Donnel MP, Cleary MP, Keane WF. Treatment of hyperlipidemia reduces glomerular injury in obese Zucker rats. *Kidney Int* 1988; **33**: 667–672.
17 Li MC, He SH. IL-10 and its related cytokines for treatment of inflammatory bowel disease. *World J Gastroenterol* 2004; **10**: 620–625.
18 Ito T, Okada T, Miyashita H, Nomoto T, Nonaka-Sarukawa M, Uchibori R *et al.* Interleukin-10 expression mediated by an adeno-associated virus vector prevents monocrotaline-induced pulmonary arterial hypertension in rats. *Circ Res* 2007; **101**: 734–741.
19 Alderson NL, Chachich ME, Youssef NN, Beattie RJ, Nachtigal M, Thorpe SR *et al.* The AGE inhibitor pyridoxamine inhibits lipemia and development of renal and vascular disease in Zucker obese rats. *Kidney Int* 2003; **63**: 2123–2133.
20 Tsilibary EC. Microvascular basement membranes in diabetes mellitus. *J Pathol* 2003; **200**: 537–546.
21 Caramori ML, Kim Y, Huang C, Fish AJ, Rich SS, Miller ME *et al.* Cellular basis of diabetic nephropathy: 1. Study design and renal structural-functional relationships in patients with long-standing type 1 diabetes. *Diabetes* 2002; **51**: 506–513.
22 Akimoto T, Ito C, Saito O, Takahashi H, Takeda S, Ando Y *et al.* Microscopic hematuria and diabetic glomerulosclerosis—clinicopathological analysis of type 2 diabetic patients associated with overt proteinuria. *Nephron Clin Pract* 2008; **109**: c119–c126.
23 Fürnsinn C, Komjati M, Madsen OD, Schneider B, Waldhäusl W. Lifelong sequential changes in glucose tolerance and insulin secretion in genetically obese Zucker rats (fa/fa) fed a diabetogenic diet. *Endocrinology* 1991; **128**: 1093–1099.
24 Sandler S, Welsh N. Interleukin-10 stimulates rat pancreatic islets *in vitro*, but fails to protect against interleukin-1. *Biochem Biophys Res Commun* 1993; **195**: 859–865.
25 Sarafidis PA, Ruilope LM. Insulin resistance, hyperinsulinemia, and renal injury: mechanisms and implications. *Am J Nephrol* 2006; **26**: 232–244.
26 Bjorn SF, Bangstad HJ, Hanssen KF, Nyberg G, Walker JD, Viberti GC *et al.* Glomerular epithelial foot processes and filtration slits in IDDM patients. *Diabetologia* 1995; **38**: 1197–1204.
27 Herbach N, Schairer I, Blutke A, Kautz S, Siebert A, Goke B *et al.* Diabetic kidney lesions of GIPR^{dn} transgenic mice: podocyte hypertrophy and the thickening of the GBM precede glomerular hypertrophy and glomerulosclerosis. *Am J Physiol Renal Physiol* 2009; **296**: F819–F829.
28 Bonnet F, Cooper ME, Kawachi H, Allen TJ, Boner G, Cao Z. Irbesartan normalizes the deficiency in glomerular nephrin expression in a model of diabetes and hypertension. *Diabetologia* 2001; **44**: 874–877.
29 Luimula P, Ahola H, Wang SX, Solin ML, Aaltonen P, Tikkanen I *et al.* Nephrin in experimental glomerular disease. *Kidney Int* 2000; **58**: 1461–1468.
30 Hollis JH, Lemus M, Evetts MJ, Oldfield BJ. Central interleukin-10 attenuates lipopolysaccharide-induced changes in food intake, energy expenditure and hypothalamic Fos expression. *Neuropharmacology* 2010; **58**: 730–738.
31 Okada T, Nomoto T, Yoshioka T, Nonaka-Sarukawa M, Ito T, Ogura T *et al.* Large-scale production of recombinant viruses by use of a large culture vessel with active gassing. *Hum Gene Ther* 2005; **16**: 1212–1218.

Recovery of neurogenic amines in phenylketonuria mice after liver-targeted gene therapy

Hiroya Yagi[a,b], Sho Sanechika[c], Hiroshi Ichinose[c], Chiho Sumi-Ichinose[d], Hiroaki Mizukami[a], Masashi Urabe[a], Keiya Ozawa[a] and Akihiro Kume[a]

Phenylketonuria (PKU) is a common genetic disorder arising from a deficiency of phenylalanine hydroxylase. If left untreated, the accumulation of phenylalanine leads to brain damage and neuropsychological dysfunction. One of the abnormalities found in hyperphenylalaninemic patients and a mouse model of PKU is an aminergic deficit in the brain. We previously showed correction of hyperphenylalaninemia and concomitant behavioral recovery in PKU mice after liver-targeted gene transfer with a viral vector. Here, we addressed whether such a functional recovery was substantiated by an improved amine metabolism in the brain. After gene transfer, brain dopamine, norepinephrine, and serotonin levels in the PKU mice were significantly elevated to normal or near-normal levels, along with systemic improvement of phenylalanine catabolism. The results of biochemical analyses validated the efficacy of PKU gene therapy in the central nervous system. *NeuroReport* **23:30–34 © 2011 Wolters Kluwer Health | Lippincott Williams & Wilkins.**

NeuroReport 2012, 23:30–34

Keywords: catecholamine, gene therapy, phenylketonuria, serotonin

[a]Division of Genetic Therapeutics, Jichi Medical University, Shimotsuke, [b]Department of Obstetrics and Gynecology, Institute of Clinical Medicine, University of Tsukuba, Tsukuba, [c]Department of Life Science, Graduate School of Bioscience and Biotechnology, Tokyo Institute of Technology, Yokohama and [d]Department of Pharmacology, School of Medicine, Fujita Health University, Toyoake, Japan

Correspondence to Dr Akihiro Kume, MD, PhD, Division of Genetic Therapeutics, Jichi Medical University, 3311-1 Yakushiji, Shimotsuke, Tochigi 329-0498, Japan Tel: +81 285 58 7402; fax: +81 285 44 8675; e-mail: kume@jichi.ac.jp

Received 1 September 2011 accepted 17 October 2011

Introduction

Phenylketonuria (PKU; OMIM 261600) is a common inherited metabolic disorder, mostly arising from a deficiency of phenylalanine hydroxylase (PAH) [1]. PAH is exclusively responsible for converting phenylalanine into tyrosine, and its deficiency results in a systemic accumulation of phenylalanine in the body. Although the mechanisms involved are not fully understood, excessive amounts of phenylalanine are toxic to the developing brain and have a negative impact on neuropsychological function in adults. Therefore, the present treatment for PKU mandates strict restrictions of dietary protein in infancy and childhood to limit phenylalanine intake, and a similar diet is recommended for life. One possible mechanism responsible for the neurological dysfunction is an aminergic deficit, as earlier studies showed drastic decreases in neurotransmitters such as dopamine, norepinephrine, and serotonin (5-hydroxytryptamine, 5-HT) in the brains of untreated PKU patients [2,3]. A similar aminergic deficit was found in a mouse model of PKU (the *Pah*^{enu2} strain) [4–7]. We and other investigators have explored the feasibility of somatic gene therapy for PKU, and have shown that recombinant adeno-associated virus (AAV) vectors can achieve long-term corrections of hyperphenylalaninemia (HPA) in *Pah*^{enu2} mice [8–10]. We also demonstrated a behavioral recovery in the treated animals, indicating that some brain functions benefited from this approach [8]. In the present study, we addressed whether liver-targeted gene therapy for PKU would reinstate the metabolism of neurogenic amines, thereby improving homeostasis and the function of the central nervous system.

Materials and methods

Animals

All the animal experiments were carried out in accordance with the institutional guidelines under protocols approved by the Institutional Animal Care and Use Committee at Jichi Medical University (Shimotsuke, Japan). PAH-deficient C57BL/6-*Pah*^{enu2} mice (PKU mice, −/−) were homozygous for the same *Pah*^{enu2} mutation as that described in the original BTBR-*Pah*^{enu2} strain [4,5], but had been bred and backcrossed on the C57BL/6J background. Genotyping for the presence of the *Pah*^{enu2} mutation was performed by PCR analysis of tail biopsy DNA [9]. All the mice were maintained on standard mouse chow (CE-2 from Clea, Tokyo, Japan). Blood was collected from the tail veins on a filter paper for newborn mass screening (No. 545 from Advantec Toyo, Tokyo, Japan), and blood phenylalanine concentrations were determined by an enzymatic fluorometric assay using an Enzaplate PKU-R kit (GE Healthcare, Tokyo, Japan) and a Fluoroskan Ascent FL plate reader (Labsystems, Helsinki, Finland) [8,9]. *In-vivo* phenylalanine oxidation was evaluated by a noninvasive breath test using [1-^{13}C]L-phenylalanine [9,11].

In-vivo gene transfer

The construction and preparation of the AAV8-pseudotyped self-complementary AAV vector for PKU (scAAV8/

0959-4965 © 2011 Wolters Kluwer Health | Lippincott Williams & Wilkins DOI: 10.1097/WNR.0b013e32834e3a87

LP1-mPAH) has been described previously [9]. 1×10^{11} vector genomes of the recombinant AAV were dissolved in 0.5 ml of saline and injected into the peritoneal cavity of a PKU mouse at 8 weeks of age.

Brain sampling and biochemical analysis

Mice were killed by cervical dislocation, and the removed brain was immediately frozen in liquid nitrogen and stored at −80°C until used. The brain was homogenized in 10 volumes of 0.2 M of perchloric acid containing 0.1 mM of EDTA for deproteination. Protein concentrations were determined using a DC protein assay kit (Bio-Rad, Hercules, California, USA). Catecholamine and 5-HT levels were measured by high-performance liquid chromatography using an electrochemical detector ECD-100 (EICOM, Kyoto, Japan) as described elsewhere [12]. Amino acid levels were analyzed using an L-8500 amino acid analyzer (Hitachi, Tokyo, Japan). Data are presented as means ± SDs in the text and figures. An unpaired *t*-test was performed using the StatView 5.0 software for Macintosh (SAS Institute, Cary, North Carolina, USA) for comparison between two groups, and a P value of less than 0.05 was considered to be significant.

Results

Phenotypic correction after gene transfer

As shown in the original BTBR-*Pah*^{enu2} mice [9], the scAAV8/LP1-mPAH vector exhibited remarkable efficacy in restoring phenylalanine catabolism in C57BL/6-*Pah*^{enu2} mice. Before the gene transfer, PKU mice had elevated blood phenylalanine levels (28.1 ± 1.7 mg/dl; $n = 3$) compared with their heterozygous (+/−) littermates (0.3 ± 0.2 mg/dl; $n = 6$), whereas blood phenylalanine levels in heterozygous mice were indistinguishable from those in wild-type homozygous (WT, +/+) mice (0.3 ± 0.1 mg/dl; $n = 6$). After a single injection of the AAV vector to PKU mice, the blood phenylalanine concentration rapidly decreased to a near-normal level in 1 week (1.7 ± 0.8 mg/dl) and remained within the normal range from weeks 2 to 8 (Fig. 1a). In parallel, we evaluated phenylalanine-oxidizing capacity by conducting a ^{13}C-phenylalanine-loading breath test (Fig. 1b). In this assay, the production of $^{13}CO_2$ (ΔCO_2) is associated with PAH activity, although we were not able to distinguish heterozygous mice (50.6 ± 6.7‰; $n = 6$) from WT mice (52.6 ± 10.5‰; $n = 6$), presumably due to other limiting factors such as phenylalanine transport and cofactor availability *in vivo*. Before the gene transfer, PKU mice produced very little, if any, ΔCO_2 (2.0 ± 1.1‰; $n = 3$). One week post-AAV injection, ΔCO_2 was increased to 2/3 of the control level (29.9 ± 1.1‰) and the value gradually increased to a near-normal level (41.8 ± 3.5‰ at week 8).

The AAV-treated PKU mice ($n = 3$) were euthanized at week 8 after injection along with heterozygous littermates ($n = 6$) and age-matched, untreated PKU mice ($n = 4$) for further analysis. First, we measured the whole brain weight of these animals (Fig. 1c). As reported [13], the weight of the brain in untreated PKU mice was significantly decreased compared with the control level (343 ± 15 vs. 481 ± 33 mg; $P = 0.00005$). In contrast, the brains of AAV-treated PKU animals regained weight significantly (431 ± 26 mg; $P = 0.0023$ vs. untreated PKU), reaching a level comparable level to that in heterozygous mice ($P = 0.55$).

Amino acid analysis

In the amino acid analysis, we confirmed that the untreated PKU mice had a marked imbalance of phenylalanine and tyrosine in the brain [13] (Fig. 2a). The phenylalanine content was nearly 10 times that of heterozygous mice (6.24 ± 0.81 vs. 0.66 ± 0.08 nmol/mg protein; $P = 0.0008$), whereas the tyrosine content was lower (0.31 ± 0.08 vs. 0.77 ± 0.09 nmol/mg protein; $P = 0.0005$). In the AAV-treated PKU mice, the amount of phenylalanine in the

Fig. 1

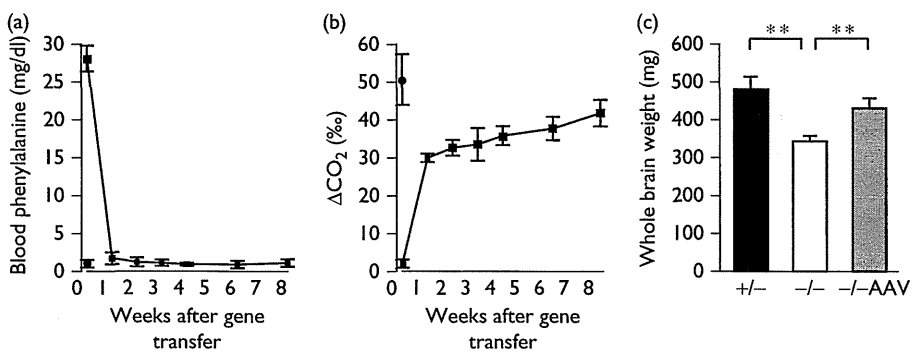

Phenotypic correction in phenylketonuria (PKU) mice after gene transfer. (a) Blood phenylalanine levels in adeno-associated virus (AAV)-treated PKU mice (squares) and heterozygous controls (circle). (b) $^{13}CO_2$ production (ΔCO_2) by AAV-treated PKU mice (squares) and heterozygous controls (circle) in a [1-^{13}C]L-phenylalanine-loading test. (c) Whole brain weights of heterozygous control (+/−), untreated PKU (−/−), and AAV-treated PKU (−/−AAV) mice. Data are shown as the mean ± SD. **P<0.01.

brain was decreased (1.04 ± 0.50 nmol/mg of protein; $P = 0.001$ vs. untreated PKU) in accordance with that in blood. The treated mice also had increased levels of tyrosine, but the elevation was not significant because one animal had a supranormal tyrosine content (1.55 nmol/mg of protein) that resulted in a relatively large SD for this group. As for tryptophan, the untreated PKU mice had a lower average level (0.12 ± 0.05 nmol/mg protein) than the heterozygous and AAV-treated mice (0.21 ± 0.11 and 0.28 ± 0.13 nmol/mg of protein, respectively), but the difference was not significant as reported previously [7].

Monoamine neurotransmitters and metabolites

The levels of catecholamines, serotonin, and metabolites are summarized in Table 1. We confirmed that the amounts of dopamine, norepinephrine, and 5-HT in the untreated PKU mice were significantly decreased compared with those in the heterozygous controls ($P = 0.004$, 0.0005, and 0.00008, respectively) [6,7]. Eight weeks after gene transfer, such aminergic deficits were markedly ameliorated ($P = 0.022$, 0.0007, and 0.0004 vs. untreated PKU, respectively; Fig. 2b). Accordingly, the levels of some catecholamine metabolites increased in the AAV-treated mice. In PKU mice, 3-4-dihydroxyphenylacetic acid decreased significantly compared with the heterozygous controls, and it recovered partly after gene transfer. 3-methoxytyramine (3-MT) content in PKU mice was not significantly lower than that in the heterozygous controls, but it may have actually been lower compared with WT homozygotes [6]. Otherwise, a compensatory dopamine release to the synapse may take place in PKU mice, resulting in a relatively small 3-MT decrease. As shown in Table 1, we found a significant increase in 3-MT after gene therapy, presumably due to an improved dopamine synthesis. In contrast, homovanillic acid did not increase after gene transfer ($P = 0.749$ vs. PKU; $P = 0.023$ vs. heterozygous). Overall, we assumed that catecholamine synthesis in the AAV-treated mice was restored to approximately 80–90% of the level in heterozygous mice. Similarly, the levels of serotonin and its metabolite 5-hydroxyindoleacetic acid recovered to 60–70% of those in heterozygous mice ($P = 0.039$ for 5-HT and $P = 0.092$ for 5-hydroxyindoleacetic acid).

Fig. 2

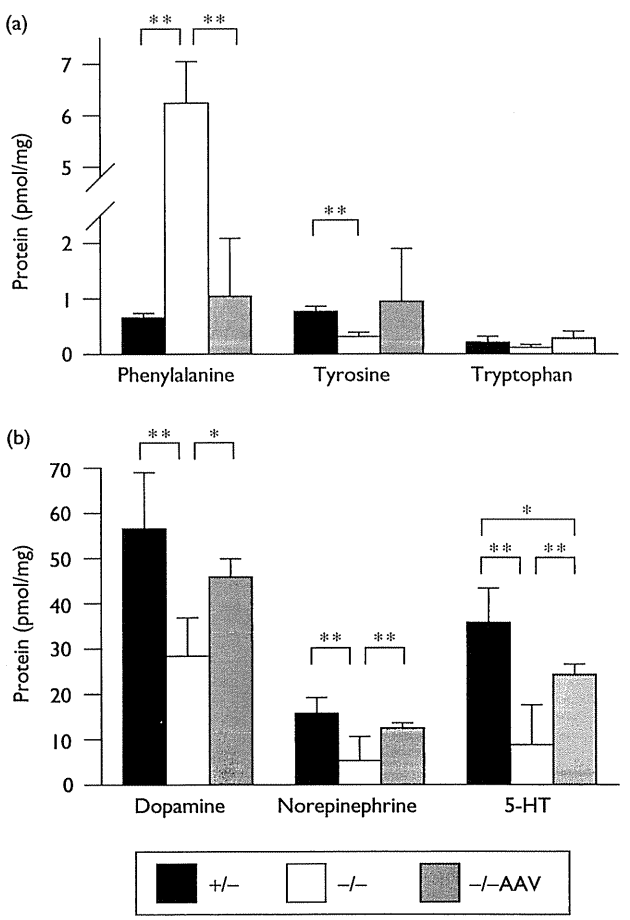

Aromatic amino acids and neurogenic amines in the phenylketonuria (PKU) mouse brain. (a) Phenylalanine, tyrosine, and tryptophan levels in the brain of heterozygous control (+/−), untreated PKU (−/−), and adeno-associated virus (AAV)-treated PKU (−/−AAV) mice. (b) Dopamine, norepinephrine, and serotonin (5-HT) levels in the brain of heterozygous control (+/−), untreated PKU (−/−), and AAV-treated PKU (−/−AAV) mice. Data are shown as the mean ± SD. *$P<0.05$, **$P<0.01$.

Discussion

The present study showed an overt reversal of the aminergic deficit in PKU mouse brain after liver-targeted gene therapy. In untreated PKU mice, HPA may disturb monoamine synthesis through at least two mechanisms. One is that excess phenylalanine may hamper t neuronal uptake of tyrosine (dopamine and norepinephrine precursor) and tryptophan (5-HT precursor) through competition for transport across the blood–brain barrier by the L-type amino acid carrier [14,15]. The other is that a high concentration of phenylalanine interferes with tyrosine hydroxylase and tryptophan hydroxylase [16,17]. For the catecholamine pathway, we observed a significant decrease in the amount of tyrosine in PKU mice, which may play some role in the dopamine and norepinephrine deficit. However, Joseph and Dyer [18] reported an increase in dopamine despite low tyrosine levels in PKU mice on a low-phenylalanine diet, which may suggest that HPA causes a lack of catecholamine primarily by inhibiting the hydroxylation of tyrosine. As for the serotonin pathway, we found a limited decrease in tryptophan in the PKU mouse brain. Pascucci *et al.* [7] found a similar decrease in tryptophan and observed a significant decrease in 5-hydroxytryptophan in the brain of PKU mice. Therefore, they speculated that HPA impedes 5-HT synthesis mainly by inhibiting tryptophan hydroxylation, which is the rate-limiting step in this pathway. We previously showed that phenylalanine acted as an inhibitor more strongly against tryptophan hydroxylase than against tyrosine hydroxylase [17], further

Table 1 Dopamine, norepinephrine, 5-hydroxytryptamine, and metabolites (pmol/mg protein) in adeno-associated virus-treated *Pah*$^{enu2/enu2}$ and control mouse brain

	Pah$^{enu2/+}$ (n=6)	*Pah*$^{enu2/enu2}$ (n=4)	*Pah*$^{enu2/enu2}$ + adeno-associated virus (n=3)
Dopamine	56.6±12.4[a]	28.4±8.5	45.9 ±4.0[a]
3-Methoxytyramine	11.9±4.6	9.9±2.1	13.7±1.2[b]
3-4-Dihydroxyphenylacetic acid	10.4±2.2[a]	4.7±1.2	7.9±1.6[b]
Homovanillic acid	41.9±12.1[b]	25.1±5.1	26.2±2.7[c]
Norepinephrine	15.7±3.5[a]	5.3±1.4	12.5±1.1[a]
5-Hydroxytryptamine	35.8±7.5[a]	8.8±2.5	24.3±2.3[a,c]
5-Hydroxyindoleacetic acid	24.3±7.9[a]	5.3±1.5	15.0±2.0[a]

Values are represented as mean±SD.
[a]$P<0.01$ vs. *Pah*$^{enu2/enu2}$.
[b]$P<0.05$ vs. *Pah*$^{enu2/enu2}$.
[c]$P<0.05$ vs. *Pah*$^{enu2/+}$.

supporting their speculation. By either mechanism, correction of HPA would reset amine metabolism and thereby improve the relevant brain function, as we demonstrated here and previously [8].

Untreated PKU patients have smaller brains, and the primary pathologic finding is hypomyelination and gliosis of central nervous system white matter. A similar pathologic change is observed in *Pah*^{enu2} mice, which may result from aberrant glial cell differentiation induced by HPA [19]. It has also been documented that cerebral protein synthesis is decreased in PKU mice, which presumably contributes to the underdevelopment and degeneration of the PKU brain [13]. We observed a marked recovery in brain weight in the PKU mice only 8 weeks after gene transfer. Correction of HPA may facilitate protein synthesis and reset glial cell plasticity to reconstitute myelin. In addition, it may reduce oxidative stress and induce neuronal regeneration as shown by Embury *et al.* [20].

The results demonstrate that liver-targeted gene therapy for PKU would restore the structural and biochemical fitness of the brain. Current gene transfer technology has achieved a partial reconstitution of coagulation factor IX in the human liver to ameliorate hemophilia B [21]. Further development should lead to broader applications of this modality including PKU. Preventing HPA without a restrictive diet would make it easier to meet nutritional requirements for the physical and neuronal development of patients as well as to maintain sociopsychological well-being.

Conclusion

Liver-targeted gene therapy for PKU reverses the aminergic deficit in the brain and improves the neuropsychological function.

Acknowledgements

The authors thank Mr. Sho Shimaguchi (Tokyo Institute of Technology) for assisting with brain amine analysis and Prof. Kazunao Kondo (Fujita Health University) for assisting with amino acid analysis. They also thank Prof. Hiroyuki Yoshikawa and Dr. Hiromi Hamada (University of Tsukuba) for enthusiastic support and thoughtful discussion. This work was supported in part by Grants-in-Aid for Scientific Research from the Ministry of Education, Culture, Sports, Science and Technology, Japan (20591230).

Conflicts of interest

There are no conflicts of interest.

References

1 Scriver CR, Kaufman S. Hyperphenylalaninemia: phenylalanine hydroxylase deficiency. In: Scriver CR, Beaudet AL, Sly WS, Valle D, editors. *The metabolic and molecular bases of inherited disease.* 8th ed New York: McGraw-Hill. 2001; pp. 1667–1724.
2 McKean CM. The effects of high phenylalanine concentrations on serotonin and catecholamine metabolism in the human brain. *Brain Res* 1972; **47**:469–476.
3 Güttler F, Lou H. Dietary problems of phenylketonuria: effect on CNS transmitters and their possible role in behavior and neuropsychological function. *J Inherit Metab Dis* 1986; **9 (Suppl 2)**:169–177.
4 Shedlovsky A, McDonald JD, Symula D, Dove WF. Mouse models of human phenylketonuria. *Genetics* 1993; **134**:1205–1210.
5 McDonald JD, Charlton CK. Characterization of mutations at the mouse phenylalanine hydroxylase locus. *Genomics* 1997; **39**:402–405.
6 Puglisi-Allegra S, Cabib S, Pascucci T, Ventura R, Cali F, Romano V. Dramatic brain aminergic deficit in a genetic mouse model of phenylketonuria. *NeuroReport* 2000; **11**:1361–1364.
7 Pascucci T, Ventura R, Puglisi-Allegra S, Cabib S. Deficits in brain serotonin synthesis in a genetic mouse model of phenylketonuria. *NeuroReport* 2002; **13**:2561–2564.
8 Mochizuki S, Mizukami H, Ogura T, Kure S, Ichinohe A, Kojima K, *et al.* Long-term correction of hyperphenylalaninemia by AAV-mediated gene transfer leads to behavioral recovery in phenylketonuria mice. *Gene Ther* 2004; **11**:1081–1086.
9 Yagi H, Ogura T, Mizukami H, Urabe M, Hamada H, Yoshikawa H, *et al.* Complete restoration of phenylalanine oxidation in phenylketonuria mouse by a self-complementary adeno-associated virus vector. *J Gene Med* 2011; **13**:114–122.
10 Thöny B. Long-term correction of murine phenylketonuria by viral gene transfer: liver versus muscle. *J Inherit Metab Dis* 2010; **33**:677–680.
11 Kure S, Sato K, Fujii K, Aoki Y, Suzuki Y, Kato S, *et al.* Wild-type phenylalanine hydroxylase activity is enhanced by tetrahydrobiopterin supplementation in vivo: an implication for therapeutic basis of tetrahydrobiopterin-responsive phenylalanine hydroxylase deficiency. *Mol Genet Metab* 2004; **83**:150–156.
12 Sumi-Ichinose C, Urano F, Kuroda R, Ohye T, Kojima M, Tazawa M, *et al.* Catecholamines and serotonin are differently regulated by tetrahydrobiopterin: a study from 6-pyruvoyltetrahydropterin synthase knockout mice. *J Biol Chem* 2001; **276**:41150–41160.
13 Smith CB, Kang J. Cerebral protein synthesis in a genetic mouse model of phenylketonuria. *Proc Natl Acad Sci USA* 2000; **97**: 11014–11019.
14 Shulkin BL, Betz AL, Koeppe RA, Agranoff BW. Inhibition of neutral amino acid transport across the human blood-brain barrier by phenylalanine. *J Neurochem* 1995; **64**:1252–1257.

15 Pietz J, Kreis R, Rupp A, Mayatepek E, Rating D, Boesch C, *et al.* Large neutral amino acids block phenylalanine transport into brain tissue in patients with phenylketonuria. *J Clin Invest* 1999; **103**:1169–1178.
16 Curtius HC, Niederwiesser A, Viscontini M, Leimbacher W, Wagmann H, Blehova B, *et al.* Serotonin and dopamine synthesis in phenylketonuria. *Adv Exp Med Biol* 1981; **133**:277–291.
17 Ogawa S, Ichinose H. Effect of metals and phenylalanine on the activity of human tryptophan hydroxylase-2: comparison with that on tyrosine hydroxylase activity. *Neurosci Lett* 2006; **401**:261–265.
18 Joseph B, Dyer CA. Relationship between myelin production and dopamine synthesis in the PKU mouse brain. *J Neurochem* 2003; **86**:615–626.
19 Dyer CA, Kendler A, Philibotte T, Gardiner P, Cruz J, Levy HL. Evidence for central nervous system glial cell plasticity in phenylketonuria. *J Neuropath Exp Neur* 1996; **55**:795–814.
20 Embury JE, Charron CE, Martynyuk A, Zori AG, Liu B, Ali SF, *et al.* PKU is a reversible neurodegenerative process within the nigrostriatum that begins as early as 4 weeks of age in *Pah*^{enu2} mice. *Brain Res* 2007; **1127**:136–150.
21 Nathwani AC, Rosales C, McIntosh J, Riddel A, Rustagi P, Galder B, *et al.* Early clinical trial results following administration of a low dose of a novel self complementary adeno-associated viral vector encoding human factor ix in two subjects with severe haemophilia B. *Hum Gene Ther* 2010; **21**:1362.

Journal of Thrombosis and Haemostasis, **10**: 81–89 DOI: 10.1111/j.1538-7836.2011.04549.x

ORIGINAL ARTICLE

Recombinant factor VIIa analog (vatreptacog alfa [activated]) for treatment of joint bleeds in hemophilia patients with inhibitors: a randomized controlled trial

ERICH V. DE PAULA,* KAAN KAVAKLI,† JOHNNY MAHLANGU,‡ YASMIN AYOB,§ STEVEN R. LENTZ,¶ MASSIMO MORFINI,** LÁSZLÓ NEMES,†† SILVA Z. ŠALEK,‡‡ MIDORI SHIMA,§§ JERZY WINDYGA,¶¶ SILKE EHRENFORTH*** and AMPAIWAN CHUANSUMRIT††† FOR THE 1804 (ADEPT™1) INVESTIGATORS[1]

**Hematology and Hemotherapy Center, University of Campinas, São Paulo, Brazil; †Department of Hematology, Ege University Medical Faculty, Children's Hospital, Bornova, Izmir, Turkey; ‡Charlotte Maxeke Johannesburg, Academic Hospital, Haemophilia Comprehensive Care Centre, Johannesburg, South Africa; §National Blood Center, Kuala Lumpur, Malaysia; ¶University of Iowa, Iowa City, IA, USA; **Centro Emofilia, Azienda Ospedaliera Careggi, Firenze, Italy; ††National Hemophilia Center, State Health Center, Budapest, Hungary; ‡‡Division of Hematology, Clinical Hospital Center, Zagreb, Croatia; §§Nara Medical University Hospital, Nara, Japan; ¶¶Department of Disorders of Hemostasis and Internal Medicine, Institute of Hematology and Transfusion Medicine, Warsaw, Poland; ***Medical and Science, Novo Nordisk A/S, Søborg, Denmark; and †††Hematology-Oncology Division, Department of Pediatrics, Faculty of Medicine, Ramathibodi Hospital, Mahidol University, Bangkok, Thailand*

To cite this article: De Paula EV, Kavakli K, Mahlangu J, Ayob Y, Lentz SR, Morfini M, Nemes L, Šalek SZ, Shima M, Windyga J, Ehrenforth S, Chuansumrit A, for the 1804 (adept™1) investigators. Recombinant factor VIIa analog (vatreptacog alfa [activated]) for treatment of joint bleeds in hemophilia patients with inhibitors: a randomized controlled trial. *J Thromb Haemost* 2012; **10**: 81–9.

Summary. *Background:* A recombinant factor VIIa analog (NN1731; vatreptacog alfa [activated]) was developed to provide safe, rapid and sustained resolution of bleeds in patients with hemophilia and inhibitors. *Patients/Methods:* This global, prospective, randomized, double-blinded, active-controlled, dose-escalation trial evaluated and compared one to three doses of vatreptacog alfa at 5, 10, 20, 40, and 80 μg kg^{-1} with one to three doses of recombinant FVIIa (rFVIIa) at 90 μg kg^{-1} in the treatment of acute joint bleeds in hemophilia patients with inhibitors. The primary endpoint comprised adverse events; secondary endpoints were evaluations of immunogenicity, pharmacokinetics, and efficacy. *Results and Conclusions:* Overall, 96 joint bleeds in 51 patients (> 12 years of age) were dosed. Vatreptacog alfa was well tolerated, with a low frequency of adverse events. No immunogenic or thrombotic events related to vatreptacog alfa were reported. A high efficacy rate of vatreptacog alfa in controlling acute joint bleeds was observed; 98% of bleeds were controlled within 9 h of the initial dose in a combined evaluation of 20–80 μg kg^{-1} vatreptacog alfa. The efficacy rate observed for rFVIIa (90%) is consistent with data from published clinical trials. The trial was not powered to compare efficacy, and further trials are needed to investigate the efficacy of vatreptacog alfa as compared with that of rFVIIa. The trial was registered at ClinicalTrials.gov (Registration Number: NCT00486278).

Keywords: hemophilia, inhibitors, rFVIIa analog, safety, vatreptacog alfa (activated).

Correspondence: Erich de Paula, Laboratorio de Hemostasia, Hemocentro de Campinas, Rua Carlos Chagas 480, São Paulo 13081-878, Brazil.
Tel.: +55 19 3521 8756; fax: +55 19 3521 8600.
E-mail: erich@unicamp.br

Presented in abstract form at the 52nd annual meeting of the American Society of Hematology, Orlando, FL, 6 December 2010. E. de Paula, K. Kavakli, J. Mahlangu, *et al.*; on behalf of the 1804 (ADEPT-1) Investigators. Safety and preliminary efficacy of recombinant activated FVII analog (NN1731) in the treatment of joint bleeds in congenital hemophilia patients with inhibitors. *Blood* 2010; 116(21): 719.

[1]A complete list of members of the 1804 investigators appears in Appendix S1.

Received 5 August 2011, accepted 21 October 2011

Introduction

The development of neutralizing antibodies (inhibitors) against factor (F) VIII or FIX is a serious complication of replacement therapy in patients with congenital hemophilia. The use of FVIII/FIX-bypassing agents is the preferred treatment option for acute bleeds in patients with high-responding inhibitors. Two bypassing agents are currently available to treat patients with inhibitors, recombinant FVIIa (rFVIIa) (NovoSeven®; Novo Nordisk A/S, Bagsværd, Denmark) and plasma-derived activated prothrombin complex concentrate (pd-aPCC) (FEIBA VH®; Baxter AG, Vienna, Austria). Both agents have

well-established efficacy and safety profiles. However, the hemostatic efficacy of these agents in patients with inhibitors does not reach the rates obtained with FVIII or FIX replacement therapy in patients without inhibitors [1–3], and may display considerable intraindividual and interindividual variability [4–6].

An rFVIIa analog was developed by Novo Nordisk with the aim of providing an improved bypassing agent offering more rapid, reliable and sustained resolution of acute bleeds in patients with hemophilia and inhibitors. This would be of clinical benefit, given the reduced need for retreatment of insufficiently treated bleeds, fewer venipunctures, reduced pain and consumption of hemostatic medication and analgesics, and less interruption to daily activities. The INN name of the active pharmaceutical ingredient of rFVIIa analog (formerly designated as NN1731) is 'vatreptacog alfa (activated)', and the term 'vatreptacog alfa' is used as the name of the drug.

Vatreptacog alfa is an activated recombinant human FVIIa analog produced biosynthetically with a CHO cell line cultured in serum-free medium. No raw materials or excipients of human or animal origin are used in the production of vatreptacog alfa. It is structurally similar to rFVIIa, with the exception of three amino acid substitutions (V158D, E296V, and M298Q) affecting the protease domain, resulting in increased tissue factor (TF)-independent activity as compared with wild-type FVIIa [7]. The mutations introduced into the vatreptacog alfa molecule mimic the effects of binding to TF, and allow the molecule to express greater proteolytic activity in the absence of TF than wild-type FVIIa. This translates into greater activity than rFVIIa on the surface of activated platelets. The enhanced platelet-dependent (TF-independent) activity of vatreptacog alfa was confirmed in several non-clinical studies [7–9].

Non-clinical studies indicate that vatreptacog alfa may provide effective, rapid and lasting cessation of bleeds [8–13]. On activated platelets, vatreptacog alfa shows increased enzymatic activity, resulting in faster and more pronounced thrombin generation, and subsequently faster and stronger clot formation with increased stability against fibrinolytic degradation [7–13]. Unlike rFVIIa, vatreptacog alfa normalizes the thrombin generation rate and clot formation in several models of hemophilia [8–13]. In a severe bleeding model in hemophilia A mice, vatreptacog alfa demonstrated significantly greater efficacy and faster bleeding resolution than rFVIIa, pd-aPCC, or rFVIII [13].

In the first human dose trial in healthy subjects, rapid thrombin generation was observed immediately after vatreptacog alfa administration [14]. Approximately 73% of vatreptacog alfa was eliminated in the initial phase, with a half-life of $\sim$ 20 min, and the remaining 27% was eliminated in the terminal phase, with a half-life of $\sim$ 3.1 h. A single dose of vatreptacog alfa appeared to be safe and well tolerated in doses up to 30 $\mu g\ kg^{-1}$. No serious adverse events, including immunogenic or thromboembolic events, occurred [14].

The aim of this phase 2 trial was to evaluate the safety and preliminary efficacy of vatreptacog alfa for treatment of joint bleeds in hemophilia patients with inhibitors.

Patients, materials and methods

Trial design and objectives

The trial was a prospective, global, multicenter, randomized, double-blinded, active-controlled, dose-escalation trial, conducted from June 2007 to June 2010. The objective of the trial was to evaluate the safety and preliminary efficacy of five escalating dose levels of vatreptacog alfa (one to three doses at 5, 10, 20, 40 and 80 $\mu g\ kg^{-1}$) vs. one to three doses of rFVIIa at 90 $\mu g\ kg^{-1}$ in the treatment of joint bleeds in hemophilia patients with inhibitors. The randomization ratio was 4 : 1 (vatreptacog alfa/rFVIIa) in all dose tiers. Vatreptacog alfa (activated), rFVIIa and rFVIIa placebo were manufactured by Novo Nordisk (Hillerød, Denmark), and were provided as a sterile freeze-dried powder in single-use vials of 1.2 mg to be reconstituted with 2.2 mL of sterile water for injection.

Sequential dose escalation followed safety evaluations by an independent external data monitoring committee (DMC). Patients who experienced several joint bleeds during the trial period were randomized and treated in subsequent dose tiers for a maximum of five qualifying joint bleeds.

The primary endpoint was frequency of adverse events; secondary endpoints included evaluations of immunogenicity, pharmacokinetics and efficacy of vatreptacog alfa.

The trial was performed in accordance with the Declaration of Helsinki and its amendments in force at trial initiation [15], and the International Conference on Harmonization [16] and Japanese [17] guidelines on Good Clinical Practice. The trial was registered at ClinicalTrials.gov (Number: NCT00486278).

Eligibility criteria

The trial population included adolescent and adult males above 12 years of age with congenital hemophilia A or B complicated by high-responding inhibitors to FVIII or FIX (current or historical titer above above 5 Bethesda units mL^{-1}). Furthermore, for all patients, a documented bleeding frequency of at least two joint bleeds over 6 months or four joint bleeds over 12 months was required for inclusion in the trial.

Patients were ineligible if they had a low platelet count ($<$ 50 000 μL^{-1}), active pseudotumors, advanced atherosclerotic disease, severe liver disease, coagulation disorders other than congenital hemophilia, or a history of thromboembolic events.

In order for a joint bleed to qualify for trial product administration, the following had to be fulfilled: (i) the patient should not have received any intravenous hemostatic treatment for a minimum of 5 days prior to trial product administration; and (ii) the patient should not have had any other bleeds within 7 days of onset of the qualifying joint bleed. Qualifying bleeds included hemorrhages into elbows, knees, and ankles.

When experiencing a qualifying joint bleed, the patient had to attend the clinic and receive the initial dose of trial product within 3 h (+ 30 min) of onset of bleed. If the patient could

not meet this requirement, the bleed was not eligible for treatment with trial product.

Trial procedures

All patients experiencing a qualifying joint bleed were randomly allocated to treatment (vatreptacog alfa or rFVIIa), and always to the lowest dose tier available.

The initial dose of trial product was to be administered in a hospital setting, and this was to be followed by continuous assessment of the bleed. If the bleeding was not controlled 3 h after initial trial product administration, up to two additional doses of trial product could be given (3-h dosing interval). Other hemostatic agents could be given according to the local standard of care if, according to the investigator, the bleed was not controlled with trial product. Patients remained at the clinic for at least 12 h after the initial dose for monitoring and evaluation of clinical response. Seven days after treatment, patients attended a follow-up visit for evaluation of general safety parameters and screening for formation of antibodies towards trial product. Screening for antibodies was repeated 28 days after each trial product administration.

Outcomes

Safety parameters were adverse events including thromboembolic events, laboratory safety data (hematology, coagulation-related parameters, clinical chemistry, and urinalysis), presence of antibodies against vatreptacog alfa, physical examination, and vital signs. Coagulation-related parameters (prothrombin fragment [F_{1+2}], prothrombin time [PT], activated partial thromboplastin time [aPTT], D-dimers, and fibrinogen) were measured predose, and 10 min, 30 min, 1 h, 3 h, 8 h and 12 h postdose.

PT analysis was performed with STA Stago®, with STA-neoplastin and calcium as reagents. aPTT analysis was performed with Pathrombin SL reagents (Dade Behring, Deerfield, IL, USA). D-dimer levels were measured by ELISA: VIDAS® D-Dimer ExclusionTM (bioMérieux, Marcy l'Etoile, France). F_{1+2} was measured by ELISA: Enzygnost® F_{1+2} (monoclonal; Dade Behring). Fibrinogen levels were measured with the STA Stago®–Clauss method.

Samples for anti-vatreptacog alfa and anti-rFVIIa antibody screening were measured with a screening assay for detection of binding antibodies and a functional assay for detection of neutralizing antibodies. A radioimmunoassay with an ^{125}I-labeled vatreptacog alfa/rFVIIa tracer was used to measure binding antibodies. The presence of antibodies was confirmed by inhibition with excess unlabeled vatreptacog alfa or rFVIIa. Antibody-positive samples were characterized with in vitro clotting assays for vatreptacog alfa and FVII neutralizing antibodies.

Blood sampling for assessment of the pharmacokinetic profile was obtained in a subset of patients enrolled in dose tiers 3, 4 and 5 predose and at intervals up to 12 h postdose (24 h in the United States). The FVIIa activity was determined with a one-stage clotting assay, using the Staclot® VIIa-rTF assay, and an ACL Advance® Analyzer (Instrumentation Laboratory, Milan, Italy), as described previously [14,18]. Standard pharmacokinetic endpoints were determined from the FVIIa activity profiles after a single intravenous injection, and included area under the curve $(AUC)_{0-t}$, AUC, mean residence time (MRT), $t_{½}$, clearance (CL) and V_{ss}, with non-compartmental methods. In order to convert the dose in μg kg^{-1} to IU kg^{-1}, the specific activities (FVIIa activity per amount of drug) of vatreptacog alfa and rFVIIa were determined in reconstituted vials.

The main preliminary efficacy endpoint was the number of bleeds successfully controlled with a single dose of trial product. Overall treatment efficacy was assessed by the need for additional hemostatic medication concomitantly with the per-protocol treatment regimen. Treatment failure was defined as bleeds where additional hemostatic medication was administered to control bleeding within 12 h of the initial dose. Assessment of efficacy also included the number of doses of trial product administered to achieve and maintain hemostatic control within the scheduled 9-h dose period, and change in pain over time after the first trial product administration.

Statistics

Data from patients exposed to at least one dose of trial product were included in the safety evaluation, and data from patients with at least one efficacy evaluation postdose were included in the efficacy evaluation.

The safety of vatreptacog alfa was based on descriptive statistics. In order to ensure an adequate number of patients for addressing the efficacy endpoints, the sample size was set to 20–25 patients per dose tier.

Statistical analyses were conducted on the efficacy endpoints. Control of bleeding with a single dose of vatreptacog alfa was analyzed by logistic regression, with treatment as a factor and target joint status and time from the start of the trial as covariates. Overall treatment efficacy within 9 h was analyzed with Fisher's exact test, as data were categorical and the success rate was high. However, it should be noted that the trial was not powered for efficacy.

Results

Characteristics of the cohort

Fifty-one male patients were randomized (Fig. 1) from 28 centers in 13 countries (see Appendix S1).

At enrollment, ages ranged from 12 to 69 years, with a mean of 28 years, and the trial population included 11 patients aged 12–17 years. The majority of eligible patients had hemophilia A (n = 48). Patient demographics and baseline assessments (including hemophilia type, inhibitor level, and bleeding episode characteristics) were well balanced in the vatreptacog alfa and rFVIIa treatment groups, and were comparable between the vatreptacog alfa dose level groups.

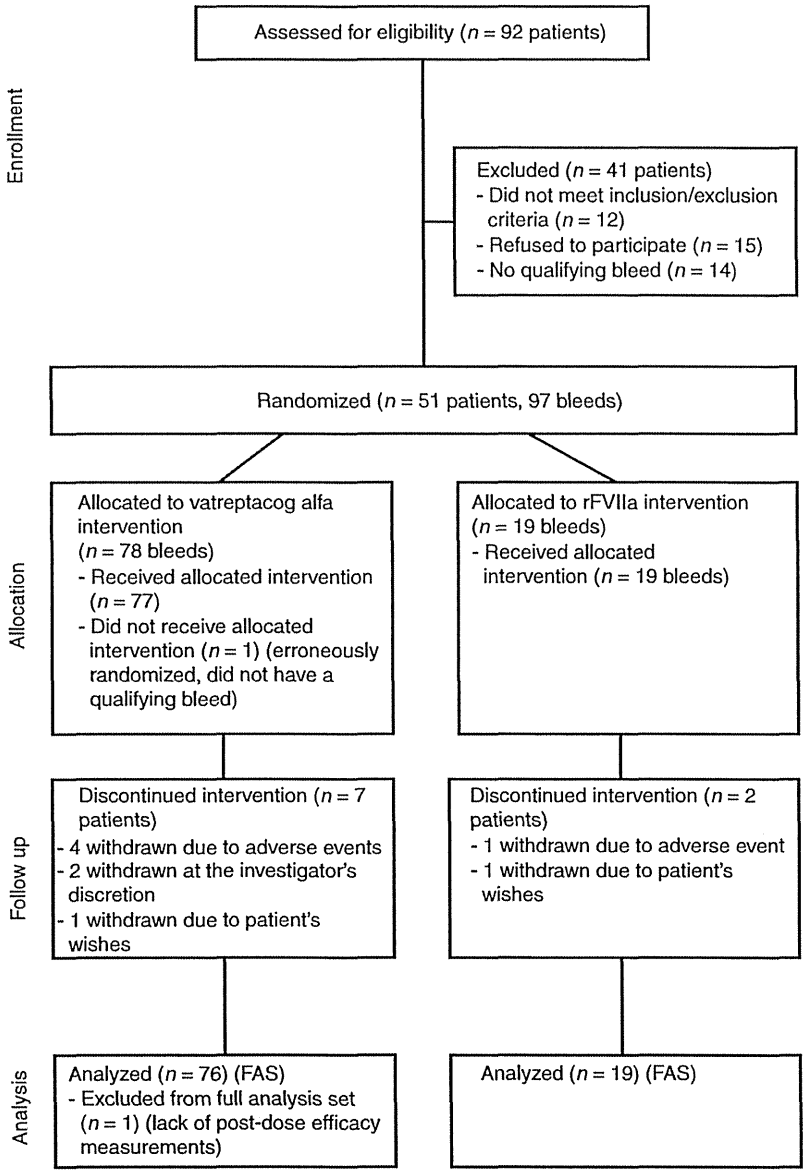

Fig. 1. CONSORT diagram showing the flow of patients and number of bleeds. FAS, full analysis set.

Differences were seen, however, in baseline joint status, which was evaluated before trial product administration for each qualifying bleed. The baseline symptoms, including swelling, pain, and loss of range of motion, were more severe for bleeds treated with rFVIIa. The proportion of target joint bleeds (defined as joints with three or more bleeds in the past 6 months) was higher among vatreptacog alfa-treated bleeds (49.4%) than among rFVIIa-treated bleeds (31.6%).

Exposure to trial products

Each dose tier was planned to enroll 25 bleeds. After DMC evaluation of the first 20 bleeds in dose tier 1, the sponsor decided to discontinue this tier, as the data indicated that this dose was subtherapeutic. Dose tier 2 included the planned 25 bleeds. Because of slow recruitment of patients into the trial, dose tiers 3 and 4 were reduced from 25 to 20 bleeds each, and dose tier 5 to 12 bleeds.

Overall, 96 bleeds were treated within the trial, including 77 bleeds with vatreptacog alfa, and 19 bleeds with rFVIIa (Fig. 1).

Fifty-one patients received at least one dose of trial product(s), and 46 of these were given vatreptacog alfa (Table 1). Two patients included in dose tier 1 received higher doses than expected, owing to errors in the reconstitution of the trial product; one patient received three doses of 19.4 μg kg^{-1} vatreptacog alfa, and one received a single dose of 26.7 μg kg^{-1} vatreptacog alfa.